where $\Gamma(k)$ is the power spectrum of $\Theta(\boldsymbol{x})$, which gives the Θ^2 amount contained in the wave vectors whose modulus are around k:

$$\int_0^\infty \Gamma(k)\,\mathrm{d}k = \frac{1}{V}\int_V \Theta^2(\boldsymbol{x})\,\mathrm{d}\boldsymbol{x} = \langle\, \Theta^2(\boldsymbol{x})\,\rangle\,,$$

where V is the volume covered by the flow.

A power spectrum following a power law,

$$\Gamma(k) \propto k^{-\sigma} \tag{4.15}$$

is said to be *local* if $1 < \sigma < 3$ (see *e.g.* [RS78, BBS84] for a detailed discussion). Only for local spectra, $S_\theta(r)$ is determined locally in the Fourier space, *i.e.* from the k in the neighbourhood of r^{-1}, and

$$S_\theta(r) \approx k\Gamma(k), \qquad \text{with } k \sim \frac{1}{r}$$

so that

$$S_\theta(r) \propto r^{\sigma-1}\,. \tag{4.16}$$

4.3.1. The power spectrum: a dynamical systems approach. In three-dimensional turbulent fluids, for large Prandtl number ν/χ_θ (ν is the kinematic viscosity of the fluid), the power spectrum obeys the Obukhov-Corrsin scaling law $\Gamma(k) \propto k^{-5/3}$ in the inertial range (where the nonlinear transfer of the fluid energy overwhelmes its molecular dissipation) [O49, C51], and the Batchelor law $\Gamma(k) \propto k^{-1}$ in the viscous convective range (where the velocity field behaviour is dominated by viscous effects but the molecular diffusion of the passive scalar is still negligible) [B59].

It is interesting to observe that Batchelor's original result was obtained by depicting the turbulent fluid, in the viscous convective range, as composed of blobs, with linear size of the order of the Kolmogorov microscale, that are subjected to the straining action of a velocity field considered regular on these length scales. Then, it is not surprising that one can derive Batchelor's result by means of ideas borrowed from the dynamical systems theory, without using phenomenological assumptions. In fact, the k^{-1} regime is a spectral property of an advected scalar which follows directly from Lagrangian chaos, and does not depend on the dimensionality d, for $d \geq 2$ [V89, CFPV90b]. Turbulent fluids and very simple flows, for instance periodic in time, exhibit this same property.

Let us consider a smooth initial condition $\Theta_0(\boldsymbol{x})$ and $N \gg 1$ particles, convected according to (4.5) by a smooth velocity field. The i-th particle is initially in $\boldsymbol{x}^{(i)}(0)$ and transports its own $\Theta^{(i)} = \Theta_0(\boldsymbol{x}^{(i)}(0))$. At time t, by the definition (4.14), one has

$$S_\theta(r) \approx N^{-2}\sum_{i,j}(\Theta^{(i)} - \Theta^{(j)})^2 P_r(\boldsymbol{x}^{(i)},\ \boldsymbol{x}^{(j)},\ t)\,, \tag{4.17}$$

where $P_r(\boldsymbol{x}^{(i)}, \boldsymbol{x}^{(j)}, t)$ is the probability density to have $|\boldsymbol{x}^{(i)} - \boldsymbol{x}^{(j)}| = r$ at time t. The dominant contribution to the sum (4.17) comes from the couples of particles with large $|\Theta^{(i)} - \Theta^{(j)}|$, that is from initially distant particles, since $\Theta_0(\boldsymbol{x})$ is smooth. In the presence of Lagrangian chaos, two particles which are initially at distance l_0 can approach up to a distance $O(r)$ after a time $t_r \sim \lambda_1^{-1} \ln(l_0/r)$. Here λ_1 is again the maximum Lyapunov exponent of the time reversed (4.7). In other terms, t_r is the typical time necessary to get a 'good mixing' on scale r: the $\Theta^{(i)}$ of the particles in a box of edge r, after this time, are distributed in the whole range of disposable values. Therefore $P_r(\boldsymbol{x}^{(i)}, \boldsymbol{x}^{(j)}, t)$ for $t > t_r$ becomes independent of r (a part from logarithmic corrections), so that

$$S_\theta(r) \sim r^\eta, \quad \text{with } \eta = 0. \tag{4.18}$$

One cannot use directly the dimensional relations (4.15) and (4.16) because the value $\eta = 0$ is out of the validity range for locality in the power spectrum. One can only assert that

$$\Gamma(k) \propto k^{-\sigma} \quad \text{with } \sigma \leq 1.$$

However, the conservation law $\int \Gamma(k)\,\mathrm{d}k = \text{constant}$ implies $\sigma \geq 1$, so that the Batchelor scaling $\sigma = 1$ follows.

4.3.2. The power spectrum: a fragmentation model. The spectral properties of a convected scalar can also be derived in the context of a fragmentation model, similar to the β-model, introduced in three-dimensional turbulence for the description of the energy cascade in the inertial range [BPPV84]. An advantage of this approach is the possibility of determining, in a simple way, the limit of validity of the k^{-1} law. Moreover, in two-dimensional turbulence, this power law is valid even in the inertial range. On the contrary, in three-dimensional fluids the extension of the range of validity of the k^{-1} law is determined by the details of the (Eulerian) turbulence.

The convection term in (4.2) is the cause of the growth of the Θ gradients. It can be regarded as the term which induces a transfer among different Fourier components of Θ, in such a way to generate a cascade of the quantity Θ^2 in the Θ Fourier space towards the large wave number harmonics, up to the wave numbers corresponding to the dissipation length (4.12), where the dissipation of the scalar fluctuations mainly occurs. This transfer mechanism is quite similar to that observed for the energy in Richardson's scenario of fully developed turbulence [R22]. In fact, one may consider Θ^2 as a quantity which is transferred across the Θ Fourier spectrum, and conserved while being transferred, according to (4.2). This means that when a Fourier component $\hat{\Theta}(k)$ is changed by the interactions between passive scalar and velocity field, at the same time other Fourier components are adjustd so that the total variation of Θ^2 is zero. If one is eager to consider a stationary state, one needs an external steady forcing on the right-hand side of (4.2), that injects Θ^2 at a constant rate χ, to balance the rate of destruction of the scalar fluctuations by molecular dissipation.

The cascade process in real space can be described by considering a sequence of length scales:

$$l_n = \beta^n l_0, \quad \text{with } \beta < 1,$$

where l_0 is the typical macroscopic length sale of the scalar gradient. At the n-th step of the fragmentation in the Θ^2 cascade, which stops at the dissipation length l_d, we have β^{-nd} boxes Λ_n of volume $(l_n)^d$. The fluctuations of the passive scalar at the scale l_n may be characterized by the quantity $\delta\theta_n$, that is the difference function

$$\delta\theta_x(r) \equiv |\Theta(\boldsymbol{x}+\boldsymbol{r}) - \Theta(\boldsymbol{x})|, \tag{4.19}$$

where $\boldsymbol{x}$ is the position of the centre of a box Λ_n and $|\boldsymbol{r}| \approx l_n$. If one has

$$\langle (\delta\theta_n)^2 \rangle = S_\theta(l_n) \propto (l_n)^\eta \tag{4.20}$$

with $0 \leq \eta < 2$, then

$$\langle (\delta\theta_n)^2 \rangle \approx k_n \Gamma(k_n), \tag{4.21}$$

and the power spectrum is

$$\Gamma(k) \propto k^{-(1+\eta)}.$$

This dimensional relation between $S_\theta(r)$ and $\Gamma(k)$ also holds for $\eta = 0$, because of the conservation law $\int \Gamma(k)\,\mathrm{d}k = \text{constant}$.

To be explicit, consider a box mother Λ_n centred around the position $\boldsymbol{x}$ of a fluid element. After a time $\tau_n(\boldsymbol{x})$ the daughter boxes Λ_{n+1} should be around $\boldsymbol{T}^{\tau_n}(\boldsymbol{x})$. On the analogy of the Kolmogorov hypothesis for the energy cascade, we assume that, on a suitable range of n, the Θ^2 transfer rate among mother and daughters is uniform in space and constant at each step of the fragmentation, that is

$$\frac{(\delta\theta_n)^2}{\tau_n} = \frac{(\delta\theta_{n+1})^2}{\tau_{n+1}} = \chi_n = \chi, \tag{4.22}$$

τ_n is the typical time needed to transfer $(\delta\theta_n)^2$ from the scale l_n to the successive scale l_{n+1}, in such a way that

$$\int (\Theta - \langle \Theta \rangle)^2 \,\mathrm{d}\boldsymbol{x} = \text{constant}. \tag{4.23}$$

The estimate of τ_n is related to the stability properties of the Lagrangian description. In fact the transfer of $(\delta\theta_n)^2$ to the scale l_{n+1} is originated by the stretching mechanism of the iso-Θ surfaces, acting on the previous scale l_n, which causes the distance between two iso-Θ surfaces, ad described in subsect. 4·1, to decrease from l_n to l_{n+1} in a time τ_n such that

$$\exp[\gamma\tau_n] = \frac{l_n}{l_{n+1}} = \beta^{-1}.$$

As there are no space fluctuations of β in this model, the decreasing of l_n does not fluctuate. This corresponds to assume the absence of temporal intermittency, in the sense used in the context of dynamical systems. Thus one has that $\gamma = \lambda_1$, the Lagrangian Lyapunov exponent of the inverse flow (4.7), that gives the mean logarithmic rate of contraction in the convecting flow. Since $\tau_n = -\ln(\beta)/\lambda_1$ is independent of n, from (4.22), (4.20) and (4.21), one gets

$$\eta = 0, \qquad \Gamma(k) \sim \frac{\chi}{\lambda_1} k^{-1}. \tag{4.24}$$

Notice that (4.22) is not just a phenomenological assumption, because it also follows from the exponential growth of the Θ gradient. Denoting τ_n as the time interval needed by two neighbouring iso-Θ surfaces in order to decrease their distance from l_n to l_{n+1}, and assuming no temporal intermittency in this process, from (4.10) one has

$$\left(\frac{\delta\theta_{n+1}}{l_{n+1}}\right)^2 = \left(\frac{\delta\theta_n}{l_n}\right)^2 \exp[2\lambda_1\tau_n]. \tag{4.25}$$

Equation (4.25) is equivalent to (4.22) with $\tau_n = \text{constant}$.

4.3.3. Numerical results. In this section numerical simulations of passive scalar fields in volume-preserving maps are reported. The maps, acting on a domain $M \subset \boldsymbol{R}^d$ with periodic boundary conditions, are used to describe the motion of particles in time-periodic velocity fields $\boldsymbol{u}(\boldsymbol{x}, t+T) = \boldsymbol{u}(\boldsymbol{x}, t)$.

The numerical simulations were done using the so-called «water-bag» method, which is largely used in hydrodynamics and plasma physics [BR70]. Because of (4.4), the time evolution of the passive scalar field $\Theta(\boldsymbol{x}, t)$ can be readily obtained from the flow of $N \gg 1$ «particles», trasported by the veocity field $\boldsymbol{u}$.

At the initial time $\Theta_0(\boldsymbol{x})$ is fixed, the N particles are distributed uniformly in the domain M and the value $\Theta^{(i)} = \Theta_0(\boldsymbol{x}^{(i)}(0))$ is associated to the i-th particle ($i = 1, \ldots, N$), initially in the position $\boldsymbol{x}^{(i)}(0)$. The particles then evolve according to a volume-preserving map. In order to calculate the spectrum $\Gamma(k)$, one needs to know the value of $\Theta(\boldsymbol{x}, n)$ on a regular lattice on M for times n, measured in units of the period T. This is achieved by partitioning the domain M into L^d cells, with $L = 2^p$ as required by the standard Fat Fourier Transform (FFT) algorithms. The value of Θ at the centre of each cell is obtained by a suitable interpolation of the $\Theta^{(i)}$ associated with the particles which are in the cell at a given time. The spectrum $\Gamma(k)$ at time n is calculated via

$$\Gamma(k) = \sum_{k \le |k'| < k+1} |\hat{\Theta}(\boldsymbol{k}', n)|^2,$$

where $\hat{\Theta}(\boldsymbol{k}, n)$ is the FFT of the Θ field.

Here results for the following two maps are presented: the standard map (2.17) ($d = 2$) and the ABC map (2.13) ($d = 3$). In the present case map (2.13)

has parameters $A_1 = A_2$, $B_1 = B_2$, $C_1 = C_2$. Figure 12 shows the time evolution of two iso-Θ lines for the map (2.17), without taking the Mod 2π, just to put in evidence the stretching. One sees that the distance between the two lines decreases in time, in agreement with the theoretical results of subsect. 1'1.

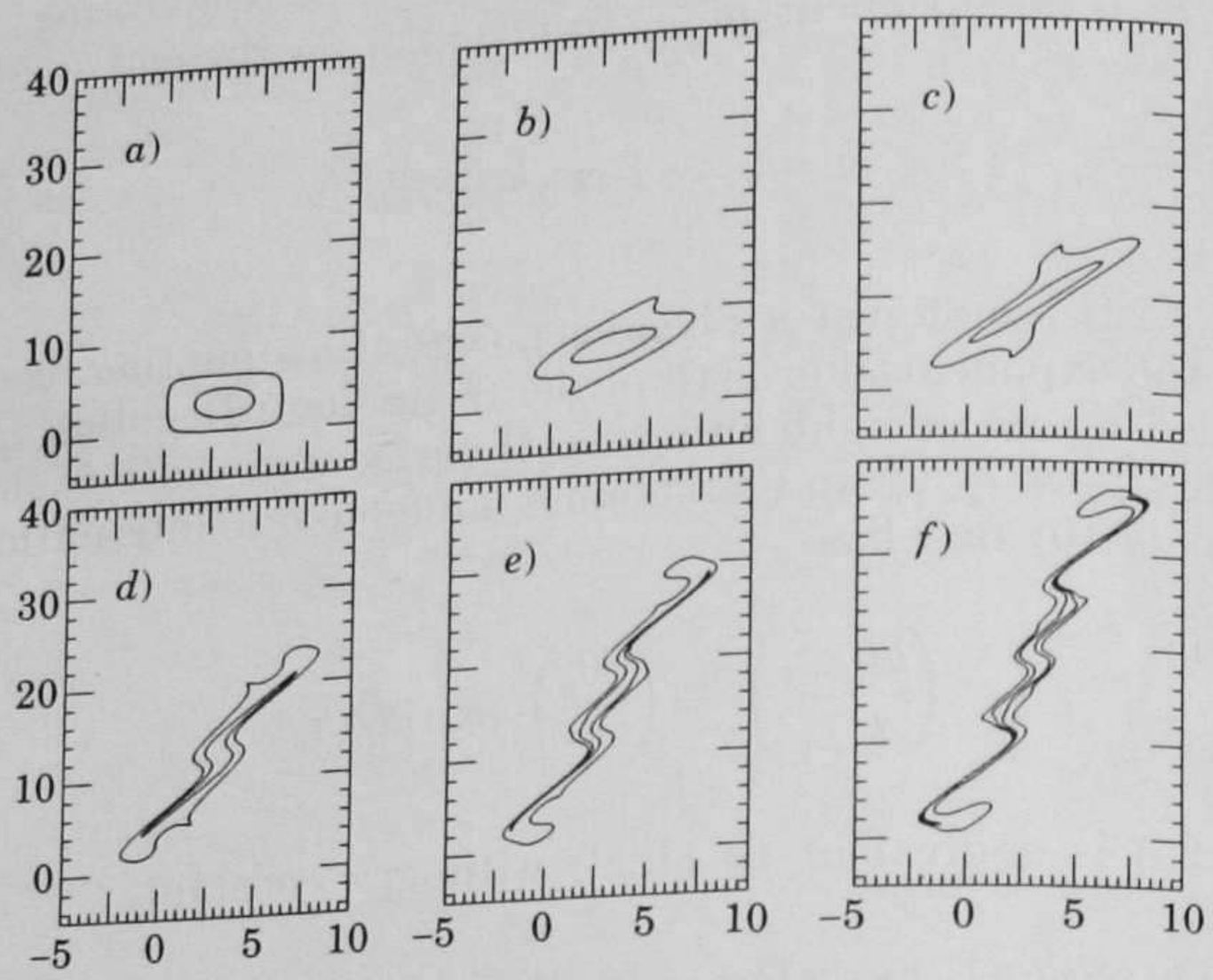

Fig. 12. – Evolution of two iso-Θ lines through 5 consecutive steps of the standard map (2.17) with $K = 0.99$. At the initial time, panel *a*), the lines are given by the equations $\sin x \sin y = \sin^2 0.5$ (external line) and $\sin x \sin y = \sin^2 2.0$ (internal line). There are no periodic boundary conditions.

Figures 13 and 14 show $\Gamma(k)$ *versus* k at different times for the two maps (2.17) and (2.13), respectively. In both cases the initial Θ_0 has a spectrum

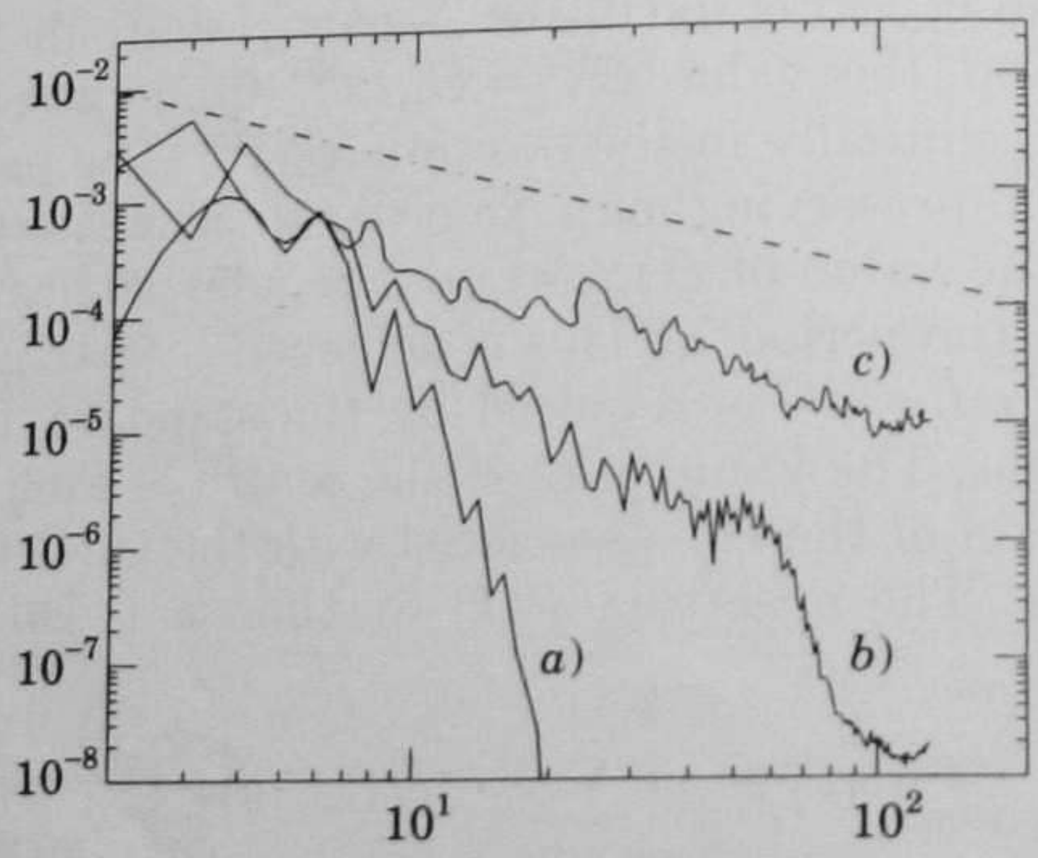

Fig. 13. – Power spectrum $\Gamma(k)$ *versus* k at different times for the standard map (2.17) with $K = 0.99$. The initial condition is $\Theta_0(x, y) = 1 + 0.2 \cos x \sin(x + y)$, $L = 256$ and the average number of particles per lattice cell is nine; the times $n = 2\ a)$, $4\ b)$, $25\ c)$ are shown. The line with slope -1 is drawn for comparison.

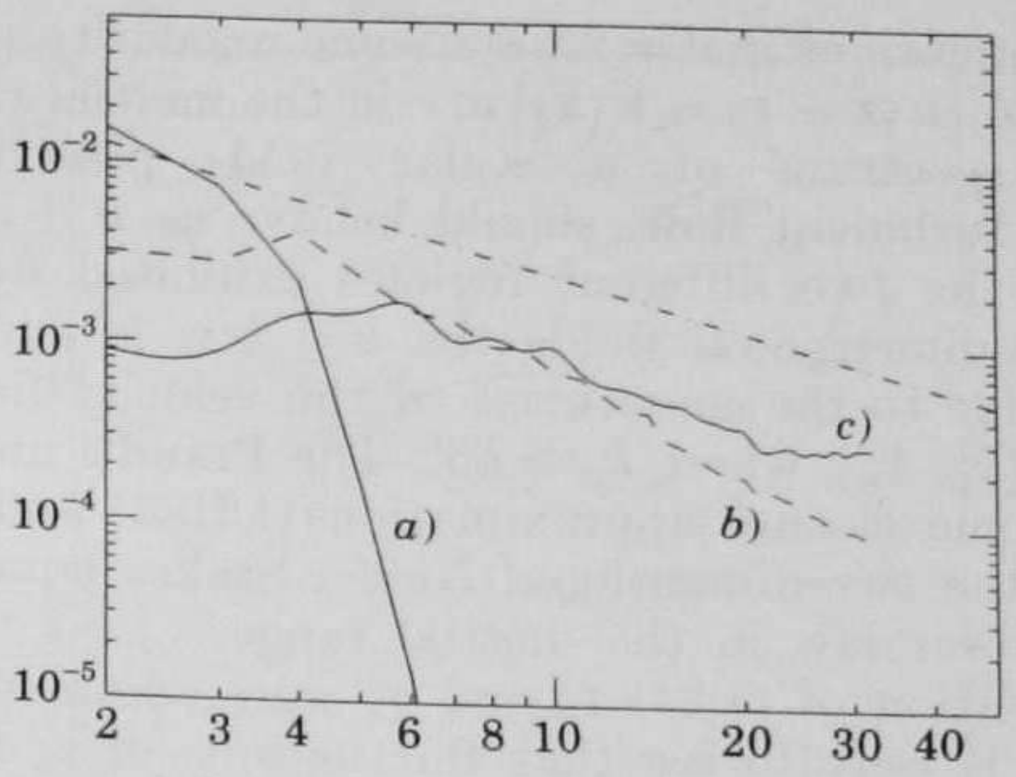

Fig. 14. – The same as fig. 13 for the ABC map (2.13) with $A = 0.5$, $B = 0.08$ and $C = 0.16$. The initial condition is $\Theta_0(x, y, z) = 1 + 0.1 \cos(x + z) + 0.2 \sin(x + y)$, $L = 64$, and the average number of particles per lattice cell is four; the times shown are $n = 3$ $(a))$, 15 $(b))$, 45 $(c))$.

concentrated in a region of small k. As time goes on, $G(t) = \langle |\nabla\Theta(\boldsymbol{x}, t)|^2 \rangle$ grows and $\Gamma(k)$ develops a k^{-1} shape. As there is no forcing, the spectrum shifts forward to large k. This is due to the conservation law (4.23) and the increasing of $G(t)$, see (4.10).

4·4. *Some remarks.* – I) To obtain the result (4.24) one has to linearize the stability equation which rules the separation between two fluid particles; and this separation has to increase at an exponential rate so as to produce a true Lagrangian chaos. These are sufficient conditions for the existence of the k^{-1} power law regime.

This implies that for turbulence in three dimensions the k^{-1} law holds only in the viscous convective subrange, where the velocity field is smoothed by the viscosity, *i.e.* $|\boldsymbol{u}(\boldsymbol{x} + \boldsymbol{r}) - \boldsymbol{u}(\boldsymbol{x})| \sim r$. This is not the case in the inertial range, where the velocity field is highly irregular and the typical velocity difference is not linear in r, *i.e.* $|\boldsymbol{u}(\boldsymbol{x} + \boldsymbol{r}) - \boldsymbol{u}(\boldsymbol{x})| \sim r^h$ with $h < 1$ ($h = 1/3$ in the Kolmogorov theory).

By the above approach, one sees that the relevance of the Eulerian turbulence is limited to determine the position of the viscous cut-off k_K, or the Kolmogorov length $l_K \approx k_K^{-1}$. This is a nontrivial task. In the Kolmogorov theory, one has $k_K \propto \mathrm{Re}^{3/4}$, but the intermittency of energy dissipation changes this power law. For instance, using homogeneous fractal models for fully developed turbulence (absolute curdling or β model), one has $k_K \propto \mathrm{Re}^{3/(1+D_F)}$, where $D_F \approx 2.8 \div 2.9$ is the fractal dimension of the set containing most of the energy dissipation, In the more complex multifractal approach [PV87b] one obtains $k_K \propto \mathrm{Re}^{1/(1+h_{\min})}$, where $h_{\min}$ is the minimum value assumed by the exponent h for the power law of the velocity differences. A rather sensible estimate is $h_{\min} = 0$ which allows good fit of the experimental structure functions for the velocity [BPPV84].

In two dimensions we are faced with a quite different scenario. It is known that in this case there exists an inertial range where the enstrophy (the integral of the square of the vorticity) cascades from larger to smaller scales. However,

the inviscid Euler equations in $d = 2$ have some regularity properties, absent in $d = 3$, which lead to $|\boldsymbol{u}(\boldsymbol{x}+\boldsymbol{r}) - \boldsymbol{u}(\boldsymbol{x})| \propto r$ in the inertial range [RS78]. Therefore the power spectrum of a scalar field, passively convected by a two-dimensional turbulent flow, should behave as k^{-1} at all length scales, and there are not the two different regimes exhibited by three-dimensional turbulence. In two-dimensional fluids the k^{-1} law is not restricted to high Prandtl numbers: due to the smoothness of the velocity field, Batchelor's law holds in the range $[k_0, k_B]$, where $k_0 \approx l_0^{-1}$. The Prandtl number only modifies the value of k_B. Some closure approximations [LH85] and numerical simulations [BBLS87] of the two-dimensional Navier-Stokes equations, provide evidence for a k^{-1} power law in the inertial range.

II) In the derivation of (4.24) τ_n and χ_n were assumed to be constant in space and in n. It is easy to see that fluctuations of τ_n and χ_n, in different boxes, can only modify the value of the constant in front of k^{-1}. In fact, the value of the scaling exponent -1 of the Batchelor law is modified only if the transfer of the passive scalar is concentrated on a set of (*active*) boxes covering a fractal stucture with dimensionality smaller than d. In terms of dynamical systems, this means that the regions of chaotic Lagrangian motion should have zero Lebesgue measure. Numerical simulations and analytical considerations show that this can happen only in extreme cases. The k^{-1} law is an exact result [K74], but the constant in front of this scaling law may be sensitive to the details of the Lagrangian motion.

III) The scaling law (4.18) admits an intuitive interpretation in terms of the fractal structure of the iso-Θ surfaces. The fractal dimension D_Θ of these surfaces and the exponent η are related by [M75, P84]

$$D_\Theta = d - \frac{\eta}{2}.$$

The k^{-1} law corresponds to surfaces (lines if $d = 2$) invading the whole space, as $D_\Theta = d$, that is the most chaotic situation. We have described a scenario where the Lagrangian chaos is the fundamental ingredient. This idea is illustrated in fig. 15 which shows one iso-Θ line in a two-dimensional fluid, with a time periodic velocity field obtained by a five-mode truncation of the Navier-Stokes equations, whose Lagrangian behaviours have been studied in subsect. **6**·5. It is impressive the similarity with the iso-Θ line computed by numerical calculations of two-dimensional fully developed turbulent flows with $\approx 10^4$ modes (see fig. 4b of [BBLS87]).

IV) We saw, in subsect. **4**·2, that the multifractal nature of $\nabla\Theta$ is revealed on scales of length $l > l_2 \sim l_0 \exp[-\gamma_{\max} t]$. For wave numbers corresponding to these scales, the scaling index of the structure function $S_\theta(r)$, and thus the exponent of the power spectrum $\Gamma(k)$, is dictated by the (multifractal) behaviour of the measure $\mathrm{d}\tilde{\mu} = |\nabla\Theta|^2 \mathrm{d}\boldsymbol{x}$. However, the onset of the k^{-1} regime for $\Gamma(k)$ occurs at length scales $l > l_1 \sim l_0 \exp[-\lambda_1 t]$, on which a good mixing has taken place and $\mathrm{d}\tilde{\mu}$, when coarse grained with such resolutions, most likely reached the uniform state. Therefore one expects the following different regions of scales:

a) $l > l_1$, where multifractality has been lost, because «good mixing properties» allows the system to forget the details of the dynamics;

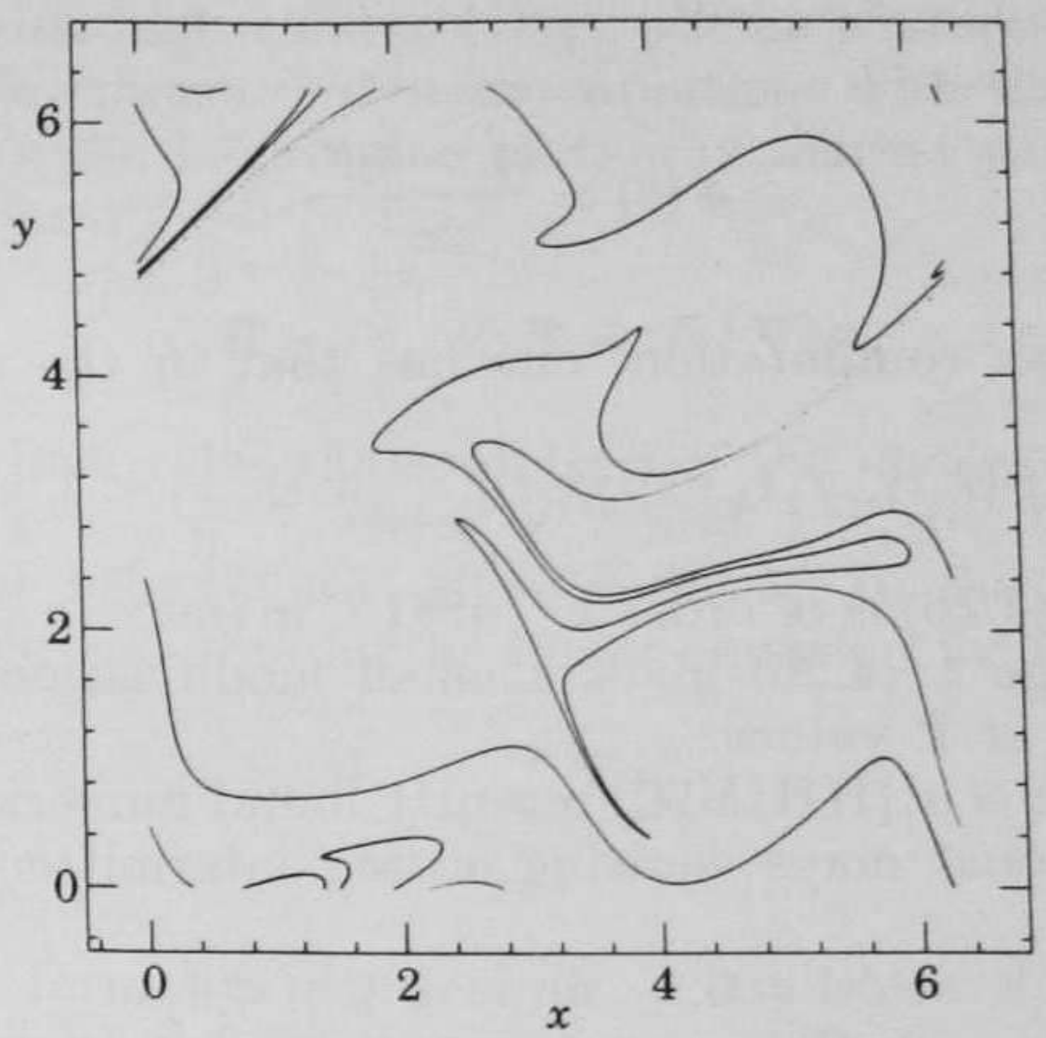

Fig. 15. – The shape of the line $(x-3.20)^2+(y-3.10)^2=(3.05)^2$, convected by the velocity field obtained as the 5-mode truncation of the $2d$ Navier-Stokes equations of sect. **3**, with $\mathrm{Re}=26.06$ (periodic regime), after ≈ 8 characteristic times (defined as $\langle(\nabla \boldsymbol{u})^2\rangle^{-1/2}$).

b) $l_2 < l < l_1$, where multifractality is at work;

c) $l < l_2$, where multifractality has not yet arrived at;

with the corresponding regimes for the power spectrum:

a) $\Gamma(k) \propto k^{-1}$ for $k < k_1 \sim l_1^{-1}$;

b) a nontrivial power law, related with the multifractal properties of the dynamical system (4.5), for $k_1 < k < k_2 \sim l_2^{-1}$;

c) an exponential decay for $k > k_2$.

Let us stress that without a steady source, regime *a*) becomes limited also from below, since, as time goes on, the power spectrum shifts toward the large k region and the low wave numbers loose their strength.

As a matter of fact, Ott and Antonsen [OA90] find for $\Gamma(k, t)$ the following expression:

$$\Gamma(k,\ t) \sim \frac{1}{kt} P\left(\frac{1}{t}\ln(k/k_0),\ t\right), \tag{4.26}$$

where $P(\gamma, t)$ is the probability density to get an effective Lyapunov exponent γ in a time interval t. $P(\gamma, t)$ can be written in terms of the function $S(\gamma)$, related via a Legendre transformation to the $L(q)$ of the dynamical system (4.7), as

$$P(\gamma,\ t) \sim \exp[-S(\gamma)t]. \tag{4.27}$$

The reader can find in subsect. **6**·3 that for $\gamma \simeq \lambda_1$, in a typical dynamical

system:

$$S(\gamma) \simeq \frac{(\gamma - \lambda_1)^2}{2\sigma^2}. \tag{4.28}$$

Then, from a simple computation, one has that in the range

$$k \in [x_1 k_0 \exp[\lambda_1 t],\ x_2 k_0 \exp[\lambda_1 t]], \quad \text{with } x_1 < 1 \text{ and } x_2 > 1,$$

the leading term of (4.26) is of order k^{-1} if $(1/t)\ln(\max[x_2, 1/x_1])$ is small. This shows that, for large t, (4.26) gives a small modification of the k^{-1} law in a very large range of k values.

Moreover, Horita *et al* [HHIM90] recently found numerical evidence that, in typical two-dimensional maps showing strong intermittency, one has

$$S(\gamma) = 0, \quad \text{for} \quad 0 < \gamma < \lambda_1.$$

In this cases (4.26) gives exactly the k^{-1} behaviour for $k < k_0 \exp[\lambda_1 t]$.

The multifractal regime of $\Gamma(k)$ thus seems rather difficult to observe in real experiments, if one does not use appropriate cares, since the diffusion coefficient introduces a natural cut-off $k_d \sim l_d^{-1} \propto \chi_\theta^{-1/2}$ which is much smaller than k_1 for reasonable times.

4·5. *The growth of vector fields: intermittency and multifractality in magnetic dynamos.* – The behaviour of a magnetic field $\boldsymbol{B}(\boldsymbol{x}, t)$ in electrically conducting fluids is of great physical relevance both in astrophysics and geophysics [W85, ZR86]. In principle, one should consider the whole set of magnetohydrodynamic equations for the velocity field $\boldsymbol{u}(\boldsymbol{x}, t)$ and the magnetic field $\boldsymbol{B}(\boldsymbol{x}, t)$. However, a simpler manner to attack the problem is to assume a prescribed velocity field as known input, unaffected by the electromagnetic field. This is the so-called kinematic dynamo problem, described by the equations

$$\begin{cases} \partial_t \boldsymbol{B} + (\boldsymbol{u} \cdot \nabla)\boldsymbol{B} = (\boldsymbol{B} \cdot \nabla)\boldsymbol{u} + \chi_B \nabla^2 \boldsymbol{B}, \\ \nabla \cdot \boldsymbol{B} = 0, \end{cases} \tag{4.29}$$

obtained from the Maxwell equations and the Ohm law for incompressible fluids, χ_B is here the magnetic-diffusivity coefficient of the fluid, inversely proportional to the conductivity. In this problem, the basic question is whether the motion can enhance a very small initial magnetic field, in the absence of external electromotive forces.

If we put $\chi_B = 0$, by taking into account that $\nabla \cdot \boldsymbol{u} = 0$ (4.29) reduces to (4.3) with $\boldsymbol{F} = \boldsymbol{B}$; then we may anticipate there will be an increase of $\boldsymbol{B}$ all over the fluid. However, because the limit $\chi_B \to 0$ is singular, the interchange of the large time limit and the small scale limit is not possible. The effect of a small but nonzero magnetic diffusivity is highly nontrivial. At the end of the section we briefly discuss this delicate point.

In the following, the statistical properties of the magnetic field on small

scales, for a fluid with high conductivity, will be characterized by exploiting the connection of the kinematic dynamo equations with the dynamical system (4.5), which describes the Lagrangian motion of marker particles in that fluid.

Consider (4.29) for $\chi_B = 0$

$$\partial_t \boldsymbol{B} + (\boldsymbol{u} \cdot \nabla)\boldsymbol{B} = (\boldsymbol{B} \cdot \nabla)\boldsymbol{u}\,, \tag{4.30}$$

and the equation which rules the evolution of the distance between two fluid particles, say $\boldsymbol{R} = \boldsymbol{x}^{(2)} - \boldsymbol{x}^{(1)}$, where $\boldsymbol{x}^{(1)}$ and $\boldsymbol{x}^{(2)}$ are the positions of the particles whose time behaviour is given by (4.5). In the limit $\boldsymbol{R} \to 0$, for the interparticle distance one obtains the linear equation for the tangent vector $\boldsymbol{z}$

$$\frac{\mathrm{d}z_k}{\mathrm{d}t} = \sum_{j=1}^{d} \frac{\partial u_k}{\partial x_j} z_j\,. \tag{4.31}$$

Equation (4.31) is formally identical to (4.30), since $\mathrm{d}/\mathrm{d}t = \partial_t + (\boldsymbol{u} \cdot \nabla)$. By considering the flow of a fluid particle, $\boldsymbol{x}(t) = \boldsymbol{T}^t \boldsymbol{x}(0)$, one can write for the evolution of the magnetic field

$$B_i(\boldsymbol{x},\ t) = \sum_{j=1}^{d} A_{ij}(\boldsymbol{x},\ t) \cdot B_j(\boldsymbol{T}^{-t}\boldsymbol{x},\ 0)$$

with

$$A_{ij}(\boldsymbol{x},\ t) = \frac{\partial x_i}{\partial (\boldsymbol{T}^{-t}\boldsymbol{x})_j}\,.$$

The behaviour of the magnetic field is thus determined by two factors: 1) the evolution of the fluid particles and 2) the rate of growth of the tangent vector, *i.e.* the separation of particles pairs.

The equivalence of (4.31) and (4.30) permits to use standard methods of dynamical systems. A magnetic field, convected by a fluid which exhibits Lagrangian chaos, will be exponentially amplified and the spatial variations in the magnetic-field amplification can be described by the generalized Lyapunov exponents $L(q)$, introduced in subsect. **4**·2; see also subsect. **6**·3. The generalized Lyapunov exponents characterize the fluctuations around λ_1 of the effective Lyapunov exponents $\gamma(\boldsymbol{x},\ t) = (1/t)\ln|z(t)|$, obtained by a measure over long but finite times. In the present context this set of exponents may be defined by the spatial averages for the $\boldsymbol{B}$-moments:

$$\langle |\boldsymbol{B}(\boldsymbol{x},\ t)|^q \rangle \sim \exp[L(q)\,t] \quad \text{for} \quad t \to \infty\,. \tag{4.32}$$

This definition is equivalent to the standard definition in terms of time averages for ergordic systems. Besides (4.32) is more appropriate for practical purposes.

We remark that an idea of generalized Lyapunov exponents has been introduced in the context of the magnetic dynamo, although limited to random velocity field, in [MRS84] and [ZMRS84].

Let us stress that since, in general, chaotic dynamical systems have a nonlinear shape of $L(q)$, for an intermittent behaviour in Lagrangian chaos, it is not necessary to consider highly irregular velocity fields, as in [ZRMS84], or strongly chaotic maps, as in [OA88] and [OA89]. As an example in fig. 16 we show the nonlinear shape of $L(q)$ obtained for the ABC map (2.13) corresponding to a three-dimensional time-periodic velocity field.

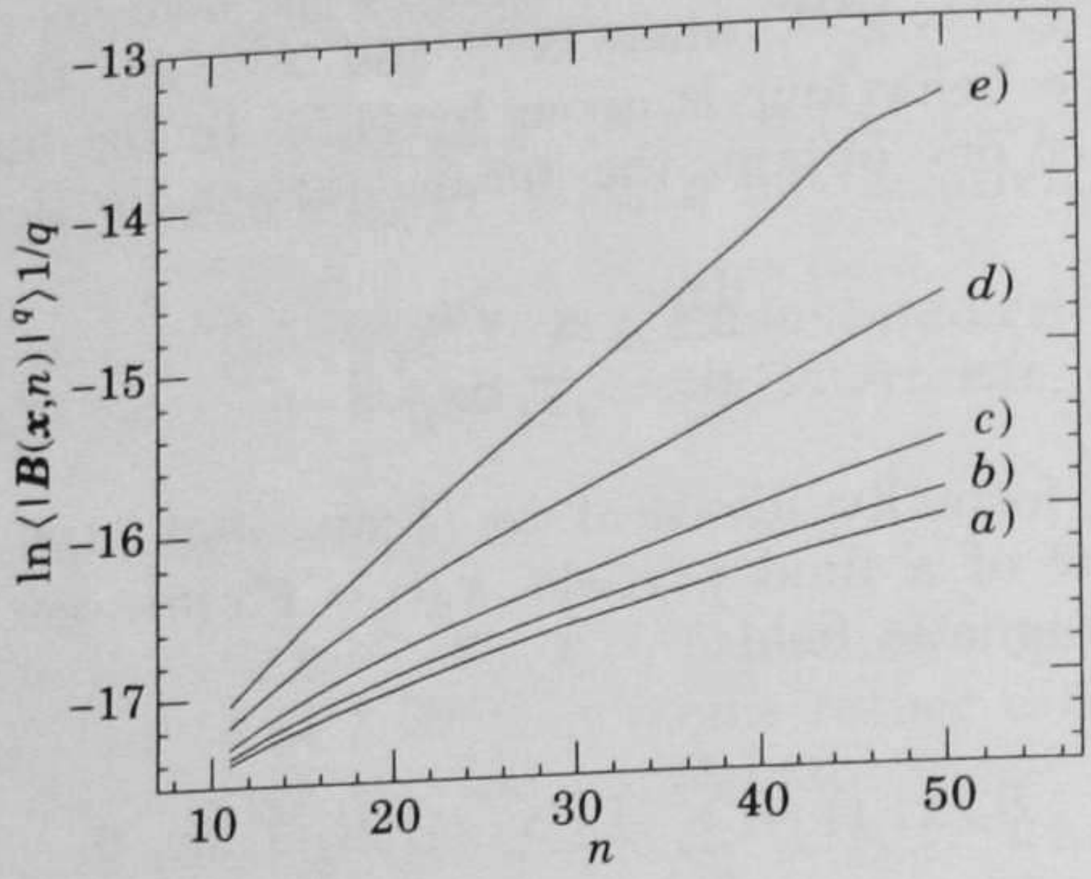

Fig. 16. – $(1/q)\ln\langle|\boldsymbol{B}(\boldsymbol{x},\,n)|^q\rangle$ *vs.* the number of steps performed, n, for the ABC map (2.13) with parameters $A=0.5$, $B=0.08$, $C=0.16$. $q=0.10$ $(a))$, 0.25 $((b))$, 0.50 $(c))$, 1.00 $(d))$, 1.50 $(e))$.

As was pointed out in the case discussed in subsect. **4**˙2, a nonlinear $L(q)$ involves the multifractality of the probability measure given by

$$\mathrm{d}\mu(x)=\frac{|\boldsymbol{B}(\boldsymbol{x},\,t)|\,\mathrm{d}^d x}{\int|\boldsymbol{B}(\boldsymbol{x},\,t)|\,\mathrm{d}^d x}, \tag{4.33}$$

where the normalization integral is over the space domain covered by the fluid.

The multifractal structure of the magnetic field is quite similar to the one of the passive scalar gradients. Multifractality and fluctuations in time of the degree of chaos are two aspects of the same problem. The relation between the spatial multifractality (*i.e.* nonconstant d_q) and temporal intermittency (*i.e.* nonlinear $L(q)$) is not simple: a detailed discussion for some chaotic systems may be found in [OA89]. However, it is easy to realize that a nonlinear $L(q)$ corresponds to a highly irregular spatial distribution for $\boldsymbol{B}(\boldsymbol{x},\,t)$. Indeed, the volume of the regions where $\boldsymbol{B}(\boldsymbol{x},\,t)\sim\exp[\gamma t]$, if $\gamma\neq\lambda_1$, vanishes as $\exp[-S(\gamma)t]$, although they give the leading contribution to $\langle|\boldsymbol{B}(x,\,t)|^q\rangle$, for $q\neq 0$. Therefore, the multifractal structure of the measure (4.33) can be observed only on very small scale, which decreases exponentially in time.

A very peculiar situation arises near the onset of Lagrangian chaos in incompressible fluids. Consider, for example, a two-dimensional system, where the Lagrangian chaos firstly appears around tiny regions of the fluids (separatrices of the stream function, see subsect. **6**˙2), embedded into large regions with

regular Lagrangian behaviour. In such a case the exponential amplification of the magnetic field is limited to the tiny chaotic regions, while one has a polynomial growth in the regular regions. As an example, the phase portrait of the most chaotic zones of the standard map (2.17) for $K = 0.5$ is shown in fig. 17. They contain the unstable fixed points of the map and those of its second iteration. The magnetic field appears to be strongly localized in these zones, as shown in fig. 18a) and 18b). As there are regular and chaotic regions which are fully disconnected, one has $L(q) = 0$ for $q < 0$, since the leading

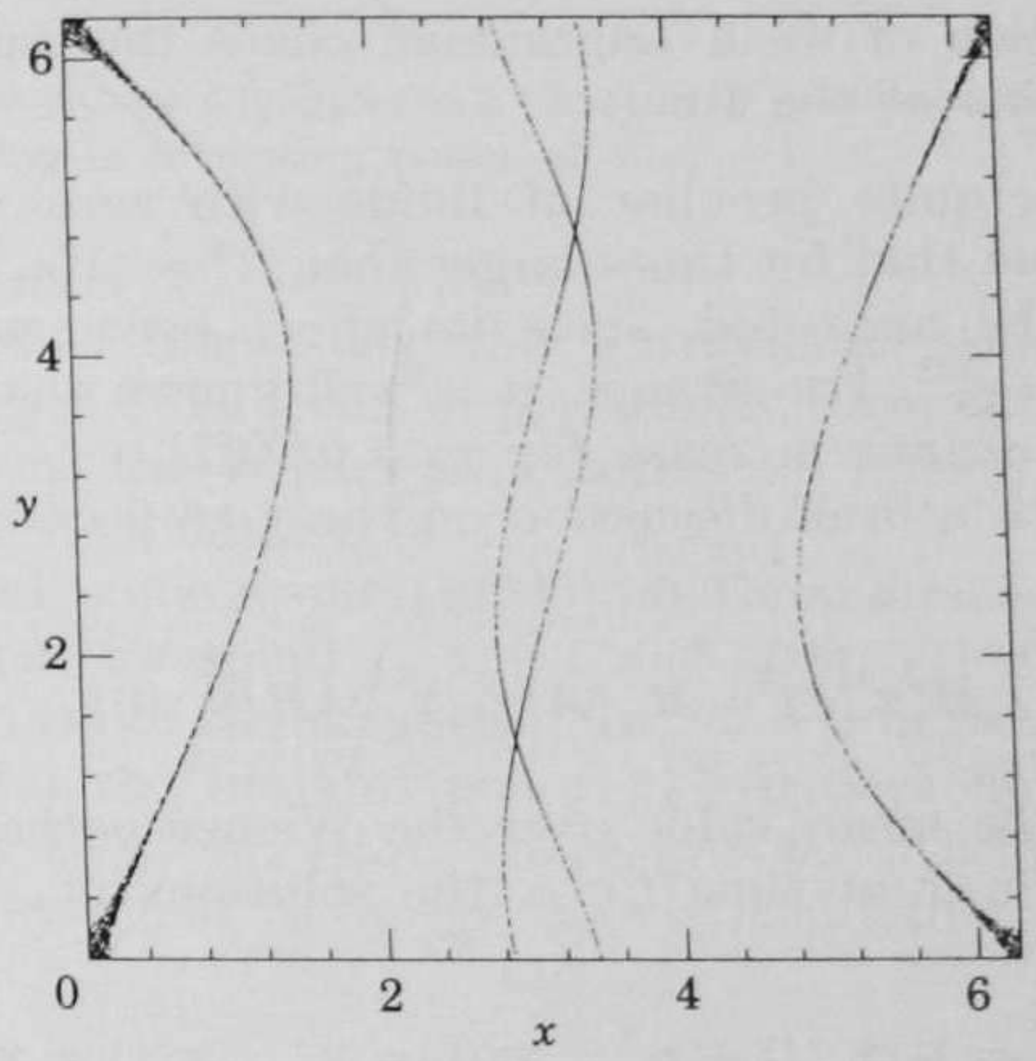

Fig. 17. – Phase portrait of the most chaotic zones of the standard map (2.17) for the parameter value $K = 0.5$.

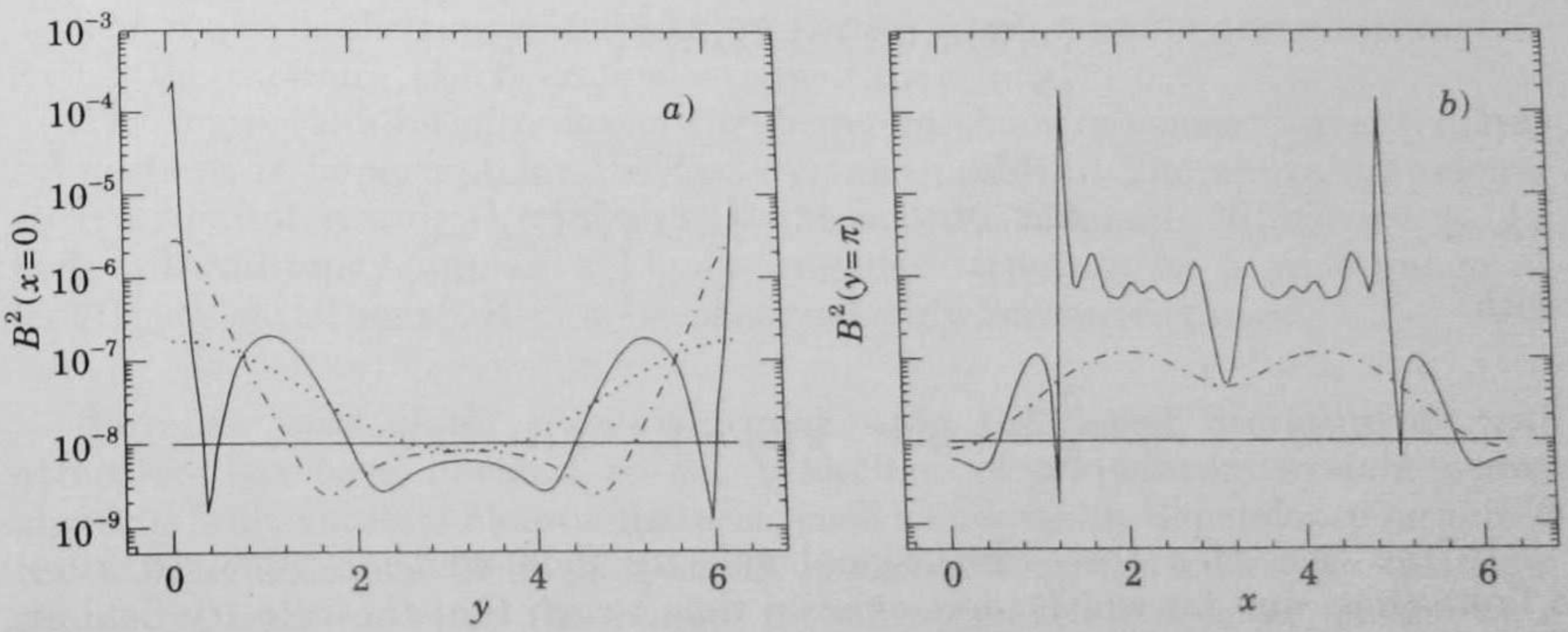

Fig. 18. – *a*) The intensity of the magnetic field *vs.* y, in the section $x = 0$, evolved by the standard map with parameter $K = 0.5$, as it appears after 2 steps (dot), 4 steps (dash-dot), 8 steps (full). The initial intensity is 10^{-8} (horizontal full line). *b*) The intensity of the magnetic field *vs.* x, in the section $y = \pi$, evolved by the standard map with parameter $K = 0.5$, as it appears after 2 steps (dash-dot), 8 steps (full). The initial intensity is 10^{-8} (horizontal full line).

contribution to the negative moments is given by the regular regions, where $\boldsymbol{B}$ does not grow exponentially. At $q = 0$ there is a jump since, by definition, $\lim_{q \to 0^+} L(q)/q = \lambda$. For $q > 0$ one should observe the usual behaviour of the function $L(q)$ due to the fluctuations of the effective Lyapunov exponent γ inside the chaotic zones.

Summing up, one has that

i) the magnetic field has a multifractal structure as a consequence of the spatial fluctuations in its exponential growth;

ii) in a situation of weak Lagrangian chaos the magnetic field concentrates in tiny regions of the fluid.

This scenario is quite peculiar of fluids with zero magnetic diffusivity coefficient. We expect that for times larger than: $t^* \sim (1/\lambda_1) \ln(\chi_B)$ the magnetic diffusivity cannot be neglected, since its effect becomes relevant on scales where $\exp[-\lambda_1 t] \sim \chi_B^{1/2}$. For istance, it is well known that in two dimensions the magnetic field cannot increase for $\chi_B \neq 0$ [Z57].

We conclude with a brief discussion on the $\chi_B \neq 0$ case. In this case (4.33) becomes [MRS84]

$$\boldsymbol{B}(\boldsymbol{x}, t) = M_x[\boldsymbol{A}(\boldsymbol{x}, \boldsymbol{y}, t)\boldsymbol{B}(\boldsymbol{y}, 0)],$$

where M_x denotes the mean value over the Wiener paths starting from $\boldsymbol{y}$ at time 0 and ending in $\boldsymbol{x}$ at time t, *i.e.* the solutions of

$$\frac{\mathrm{d}\boldsymbol{x}}{\mathrm{d}t} = \boldsymbol{u}(\boldsymbol{x}, t) + \boldsymbol{\eta}, \qquad \boldsymbol{x}(0) = \boldsymbol{y}, \qquad \boldsymbol{x}(t) = \boldsymbol{x};$$

$\boldsymbol{\eta}$ is a Gaussian process of zero mean and correlation

$$\langle \eta_i(t)\eta_j(t') \rangle = 2\chi_B \delta_{ij}\delta(t - t');$$

and

$$\boldsymbol{A}(\boldsymbol{x}, \boldsymbol{y}, t) = \exp\left[\int_0^t \mathrm{d}\tau\, \boldsymbol{a}[\boldsymbol{z}(\tau)]\right]$$

with

$$a_{ij} \equiv \frac{\partial u_i}{\partial x_j} \quad \text{and} \quad \boldsymbol{z}(0) = \boldsymbol{y}, \qquad \boldsymbol{z}(\tau) = \boldsymbol{x}.$$

In the case of a three-dimensional velocity field which is renewed after a finite time, and for which there exists a time τ such that the velocity field at time $t + \tau$ is completely uncorrelated from that at time t, it is possible to show [MRS84] that $L(q, \chi_B) \to L(q, 0)$ for $\chi_B \to 0$. Moreover $L(q, 0)$ is a non-linear function of q, indicating that, in this extreme case, the intermittency does not disappear for finite magnetic diffusivity coefficient. Figure 19 shows the expected behaviour of $L(q, \chi_B)$ as a function of χ_B.

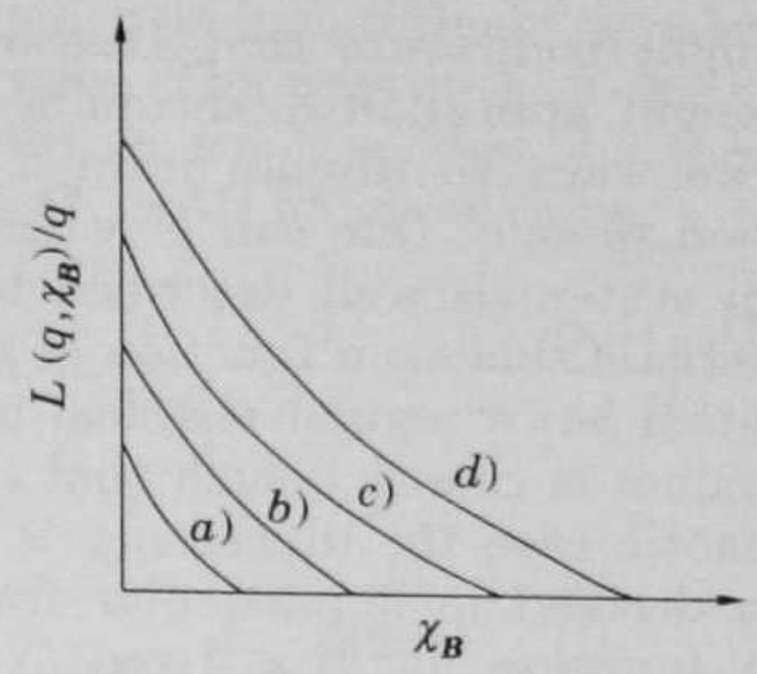

Fig. 19. – Expected behaviour of $L(q, \chi_B)/q$ as a function of χ_B; alphabetic ordering of the curves corresponds to an ordering in increasing power of q.

Note that in two dimensions the antidynamo theorem [Z57] implies $L(q, \chi_B) = 0$ for all $\chi_B \neq 0$. In terms of probability theory this is due to the fact that in two dimensions the Wiener trajectories are reflective whereas in three dimensions they are not [MRS84].

On the other hand, some results [FO90] ofr three-dimensional regular velocity fields indicate that for small χ_B and $t > t^*$, $L(q, \chi_B) = \omega q$, where ω is the exponential growth rate of the magnetic flux, $\omega = 0$ in two dimensions. Let us stress that in general the limit of ω for $\chi_B \to 0$ does not coincide with the Lyapunov exponent λ_1 of eq. (4.5), where $\chi_B = 0$. In a special class of flows (Asonov dinamical systems) it can be proved [C89] that

$$\lim_{\chi_B \to 0} \omega = L(1),$$

which can differ from λ_1.

The reflex of the zero-diffusivity properties is relevant for the multifractality of the measure (4.33) on scales larger than $\approx \chi_B^{1/2}$.

The temporal intermittency of the degree of chaos in conservative dynamical systems is important for the fast dynamo problem. The above arguments seem to be interesting even for small but nonzero magnetic diffusivity χ_B. In fact, intermittency implies a highly irregular structure on a wide range of length scales although it can be observed only on small times.

4·6. *The onset of the quantum regime.* – In the recent literature a great attention has been devoted to the behaviour of a quantum system whose classical limit exhibits chaotic features, such as a sensible dependence on initial conditions. This new field of research is called quantum chaos (or quantum chaology) and we refer the reader to some extensive reviews on the subject [Z81, B83, I90, G90].

In this subsection, we want to show that the ideas developed in the context of passive scalars can be useful to get some insight in quantum chaos. Indeed, like the diffusive equation of a scalar field, the Schrödinger equation is linear, so that an initial uncertainty on the wave function cannot grow exponentially

in time. However, one might conjecture that Lagrangian chaos of the type discussed in this section might appear in quantum systems. Without entering in this intriguing issue, we want to discuss it in a more limited case, the semi-classical approximation ($\hbar \to 0$). One can give an estimate of the time t^* up to which the quantum system is well described by the semi-classical approximation. This characteristic time as a function of $\hbar$ exhibits either a power law dependence (if the system has a regular classical behaviour), or a logarithmic one (if the classical system is chaotic), such that $t^* \to \infty$ for $\hbar \to 0$ in both cases. However, in the chaotic case the divergence is only logarithmic. These results have already been derived in a particular framework [Z81, ATI89].

If we write the wave function as $\Psi = A \exp[iS/\hbar]$, the time-dependent Schrödinger equation for a particle of mass m in a potential V becomes

$$\partial_t S + \frac{1}{m}(\nabla S)^2 + V = \frac{\hbar^2}{2m}\frac{\nabla^2 A}{A}, \tag{4.34a}$$

$$\partial_t \rho + \nabla \cdot \left(\rho \frac{\nabla S}{m}\right) = 0 \quad \text{with} \quad \rho = A^2 = |\Psi^2|. \tag{4.34b}$$

When the initial wave function $\Psi_0(\boldsymbol{x}) \equiv \Psi(\boldsymbol{x}, 0)$ is such that $(\nabla S)^2/m + V \gg (\hbar^2/2m)|\nabla^2 A|/A$, we may neglect the right-hand side of (4.34a) and we are left with the Hamilton-Jacobi equation, where S is the action and ∇S the momentum of the particle. Introducing the particle velocity field $\boldsymbol{u}(\boldsymbol{x}, t) = \nabla S/m$ and neglecting the term $O(\hbar^2)$ in (4.34a), the semi-classical limit of the above equations takes the form

$$\partial_t S + \frac{1}{m}(\nabla S)^2 + V = 0, \tag{4.35}$$

$$\partial_t \rho + (\boldsymbol{u} \cdot \nabla)\rho = -\rho \nabla \cdot \boldsymbol{u}. \tag{4.36}$$

Equation (4.35) gives the evolution of the uncoupled velocity field (in analogy with the Navier-Stokes equation), while (4.36) is very similar to (4.30) for the passive transport of $\boldsymbol{B}$ in the magnetic kinematic dynamos.

Denoting, as usual, by $\boldsymbol{T}^t$ the formal evolution operator of the equation

$$\dot{\boldsymbol{x}} = \boldsymbol{u}(\boldsymbol{x}, t) = \frac{1}{m}\nabla S(\boldsymbol{x}, t), \tag{4.37}$$

i.e. $\boldsymbol{x}(t) = \boldsymbol{T}^t \boldsymbol{x}(0)$, the solution of (4.36) may be written as

$$\rho(\boldsymbol{x}, t) = \rho_0(\boldsymbol{T}^{-t}\boldsymbol{x}) \exp\left[-\int_0^t \nabla \cdot \boldsymbol{u}(\boldsymbol{T}^{\tau - t}\boldsymbol{x}, \tau - t)\, \mathrm{d}\tau\right]. \tag{4.38}$$

The form of (4.38) allows us to repeat the arguments for the growth of $\nabla\theta$ (or $\boldsymbol{B}$) so that, if (4.37) is a chaotic system,

$$|\nabla \rho(\boldsymbol{x}, t)| \sim \exp[t\gamma(x, t)],$$

where $\gamma(\boldsymbol{x}, t)$ is related to the effective Lyapunov exponent of the flow time reversed of (4.37). For the sake of simplicity, we consider only the case

$\gamma(\boldsymbol{x}, t) \equiv \lambda$, $\forall \boldsymbol{x}, t$, although it is not difficult to take into account the fluctuations in the degree of chaos. The relevance of the term on the right hand of (4.34*a*) grows exponentially in time, so that the semi-classical approximation holds only for times $t \lesssim t^*$, with t^* given by the relation

$$E_0 \approx \frac{\hbar^2}{2m} \frac{|\nabla^2 A|}{A} \sim \frac{\hbar^2}{2m} \frac{\exp[2\lambda t^*]}{l_0^2}, \tag{4.39}$$

i.e.

$$t^* \sim \frac{1}{\lambda} \ln\left(\frac{(2mE_0)^{1/2} l_0}{\hbar}\right),$$

where l_0 and E_0 are the typical length and energy of the initial distribution.

For times $t \gtrsim t^*$, it is necessary to consider the full equations (4.34). When $t \lesssim t^*$, the chaotic nature of the probability flow reveals itself in the fact that, in spite of the linearity of the Schrödinger equation, one has

$$\rho(\boldsymbol{x}, t) - \rho(\boldsymbol{x}', t) \sim \exp[t\gamma(x, t)] \quad \text{with} \quad \boldsymbol{x} \approx \boldsymbol{x}'.$$

On the contrary, because of the linearity of the Schrödinger equation, there is no sensible dependence of $\rho(\boldsymbol{x}, t)$ upon a change of the initial condition $\rho_0(\boldsymbol{x})$. If we consider another initial condition $\tilde{\rho}_0(\boldsymbol{x})$, close to $\rho_0(\boldsymbol{x})$, and we denote with $\tilde{\rho}(\boldsymbol{x}, t)$ its evolution, we have that $\rho(\boldsymbol{x}, t) - \tilde{\rho}(\boldsymbol{x}, t)$ does not grow exponentially.

In the case of classical regular motion, $\nabla\rho$ grows only polynomially with t, so that from (4.39) one gets

$$t^* \sim \text{const}\left(\frac{(2mE_0)^{1/2} l_0}{\hbar}\right)^{\alpha},$$

with α depending on the details of the system.

To summarize, for $t \gtrsim t^*$ there is no trivial relation between the chaotic (or regular) behaviour of the classical system and the features of the corresponding quantum counterpart. However, as shown, the type of behaviour plays a central role in setting the temporal range of validity of the semi-classical approximation.

It is an open problem to understand whether a Lagrangian chaos can arise beyond the semi-classical approximation, *i.e.* in eq. (4.34) when the term proportional to $\hbar^2$ is taken into account. In this case, the equations are similar to those of a scalar field which is not passive, as for instance in the Rayleigh-Bénard convection. A theory of Lagrangian turbulence could thus become a useful tool in quantum chaos.

5. – Diffusion properties and Lagrangian chaos.

This section addresses the problem of diffusive transport in the presence of flows with Lagrangian chaos and/or molecular diffusion. The understanding of

flow-assisted diffusion is of theoretical and practical importance in diverse fields of science and engineering, ranging from mass and heat transport in geophsical flows to chemical engineering and combustion [M83]. At the fundamental level it is of interest to understand the various mechanisms that lead to transport enhancement as a fluid is driven farther from the motionless state. The reason of this enhancement is that transport is affected by the trajectories of individual fluids elements or tracers, which can be quite complex even in simple laminar flows [H66, A84].

Taking into account the molecular diffusion, the motion of a fluid element can be described by the following Langevin equation:

$$\frac{\mathrm{d}\boldsymbol{x}}{\mathrm{d}t} = \boldsymbol{u}(\boldsymbol{x},\ t) + \boldsymbol{\eta}(t)\,, \tag{5.1}$$

where $\boldsymbol{u}(\boldsymbol{x}, t)$ is the Eulerian flow velocity field at the position $\boldsymbol{x}$ at time t, and $\boldsymbol{\eta}$ is a Gaussian white noise with zero mean and

$$\langle \eta_i(t)\,\eta_j(t')\rangle = 2\chi\delta_{ij}\delta(t-t')\,. \tag{5.2}$$

The coefficient χ is the (bare) molecular diffusion coefficient. It is then clear that transport and diffusion properties are affected by the presence of Lagrangian chaos, *i.e.* the chaotic motion of a fluid element described by the deterministic equation

$$\frac{\mathrm{d}\boldsymbol{x}}{\mathrm{d}t} = \boldsymbol{u}(\boldsymbol{x},\ t)\,. \tag{5.3}$$

The dispersion of a contaminant in a fluid therefore is the result of two different effects: advection and molecular diffusion, and, in general, it is much faster than expected by considering only the latter.

Real fluids always have a certain degree of Lagrangian chaos, *e.g.*, in two-dimensional flows one just needs that the stream function is time dependent. The understanding of the diffusion process is therefore a hard task, since it may depend in a complicated way on the detailed structure of the Eulerian velocity field. Two nontrivial limit cases can, nevertheless, be immediately distinguished:

i) fully developed turbulence, where the molecular effects can be ignored on a large range of scales.

ii) fluid velocity fields where (5.3) is integrable or quasi-integrable and the degree of Lagrangian chaos is very small.

Due to the interplay of advection and molecular diffusion also the latter can be highly nontrivial.

The physics of passive diffusive transport can be characterized in simple terms by introducing an effective diffusion coefficient which contains the cumulative effects of advection and molecular diffusion. Let $\Theta(\boldsymbol{x}, t)$ be the concentration of tracers evolving in time according to the Langevin equation (5.1), then we have

$$\partial_t\Theta + \boldsymbol{u}\cdot\nabla\Theta = \chi\nabla^2\Theta\,, \tag{5.4}$$

which is nothing but the Fokker-Planck equation related to (5.1). In deriving (5.4) we have used the incompressibility condition $\nabla \cdot \boldsymbol{u} = 0$. The diffusion process takes place on time scales much longer than the characteristic microscopic time. On this time scales the evolution of $\Theta(\boldsymbol{x}, t)$ is dominated by weak long-wave disturbances. The equation for these slow modes can be derived by the usual multiple scale or «hydrodynamic» analysis [M90]. It has the form

$$\partial_t \bar{\Theta} = D_{ij} \frac{\partial^2}{\partial x_i \partial x_j} \bar{\Theta} + O((\nabla^2 \bar{\Theta})^2), \qquad i, j = 1, \ldots, d, \tag{5.5}$$

where $\bar{\Theta}$ is the concentration field averaged locally over a volume of linear dimension much larger than the typical lenght l of the velocity field. Equation (5.5) is a weak gradient expansion valid when $|\nabla \bar{\Theta}|/\bar{\Theta} \ll l^{-1}$. If we neglect the high-order term, (5.5) is the diffusion equation with an effective diffusion (tensor) D_{ij}.

From (5.5) it follows that D_{ij} measures the spreading on a very long times of a spot of tracers evolving according to (5.1). Therefore a way of computing D_{ij} is directly form the covariance tensor of the Lagrangian motion

$$D_{ij} = \lim_{t \to \infty} \frac{1}{2t} \langle (x_i(t) - \langle x_i \rangle)(x_j(t) - \langle x_j \rangle) \rangle, \qquad i, j = 1, \ldots, d. \tag{5.6}$$

Here $\boldsymbol{x}(t)$ is the position of a tracer at time t, and the average is taken over the initial position or, equivalently, over an ensemble of test particles.

Note that from (5.5) and (5.6) follows that the diffusion process is Gaussian, at least on large time and space scales. This is the typical situation, even if there exist cases where anomalous diffusion is observed, *i.e.* $\langle (x_i(t) - \langle x_i(t) \rangle)^2 \rangle \sim t^{\beta}$ with $\beta \neq 1$ [P88, WK89, OC91]. These cases will not be considered here.

The study of D_{ij} for different velocity fields $\boldsymbol{u}$ is the main object of this section. We shall consider simple problems dealing with diffusion of an impurity in a specified flow of a continuous media, without considering the origin of this field. Such a simplification of the problem is a necessary step towards the solution of the much more complex self-consistent problem and reveals, already at this idealized level, a number of nontrivial effects.

A largely used model system for a comprehensive investigation of transport is the Rayleigh-Bérnard convection, because convective flows can be created ranging from time-independent spatially periodic flows on the one hand, to turbulent flows on the other. As a result, the transport rates vary over a wide range. On one side, when the fluid is motionless, the transport is due entirely to molecular diffusion ($D_{ij} \sim \chi$). On the other extreme case, *i.e.* turbulent flows, transport is due to advection by the flow and is often described phenomenologically as enhanced diffusion.

Between these two extrema there are two important laminar regimes: time-dependent and time-independent regime. In the time-dependent regime, the trasport is dominated by advection of tracer particles across roll boundaries and the particle trajectories may be chaotic, thus $D_{ij} \neq 0$ even if $\chi = 0$. In the time-independent regime, large-scale transport is generally due to molecular

diffusion between adjacent convection rolls, so that $D_{ij} = 0$ if $\chi = 0$. However, the structure of the Eulerian velocity field can strongly modify this result, as will be discussed below.

Principal attention is paid to two-dimensional flows, since in this case the equations of motion of a fluid element are formally those of a Hamiltonian system with two degrees of freedom. Indeed in the absence of molecular diffusion (5.3) has the form

$$\frac{\mathrm{d}x}{\mathrm{d}t} = \frac{\partial \psi}{\partial y} \qquad \frac{\mathrm{d}y}{\mathrm{d}t} = -\frac{\partial \psi}{\partial x}, \tag{5.7}$$

which formally represents a Hamiltonian system, the stream function ψ playing the role of the Hamiltonian.

5·1. *Diffusion in flows with Lagrangian chaos.* – If the stream function is time dependent, the system (5.7) is nonautonomous hence, in general, nonintegrable and chaotic particle trajectories may exist. Due to the chaotic trajectories, particles may undergo a diffusion process even in very simple, *e.g.*, time-periodic laminar, Eulerian flows without the help of any type of molecular diffusion.

To illustrate this point consider the following stream function [SG88a, SG88b]:

$$\psi(x, y, t) = \frac{A}{k} \sin\left\{k\left[x + B \sin \omega t\right]\right\} W(y), \tag{5.8}$$

where A is the maximum y-velocity of the flow, k the wave number $2\pi/\lambda$ and $W(y)$ is a function that satisfies rigid boundary conditions on the surfaces $y = 0$ and $y = a$. This stream function describes single-mode, two-dimensional convection between two rigid boundaries which can be realized in time-periodic Rayleigh-Bénard convection. The direction y is identified with the vertical direction and the two surfaces $y = 0$ and $y = a$ are top and bottom surfaces of the convection cell. The term $B \sin \omega t$ represents lateral oscillations of the roll pattern of amplitude B and frequency ω that is mainly caused by the even oscillatory instability.

Due to the roll oscillations, one may expect that the trajectory of a particle near the roll separatrices could be chaotic. The numerical computation of the largest Lyapunov exponent of the Lagrangian motion confirms the presence of an extreme sensitivity on initial conditions. If we follow the evolution of a line of tracers initially located along a separatrix, see fig. 20, we may observe that it is stretched and folded, while spreading among the rolls, in a fashion typical of many chaotic dynamical systems.

It is clear that in this scenario a particle will diffuse in the x-direction. A numerical computation of the effective diffusion coefficient $D_{\parallel}$ along the channel shows a linear dependence on B for small values of $2B/\lambda$, *i.e.* with the «width» of the chaotic layer near the separatrices [SG88a, SG88b]. It is interesting that in spite of the simplicity of the model, the agreement of the numerical results with the experimental ones is quite good.

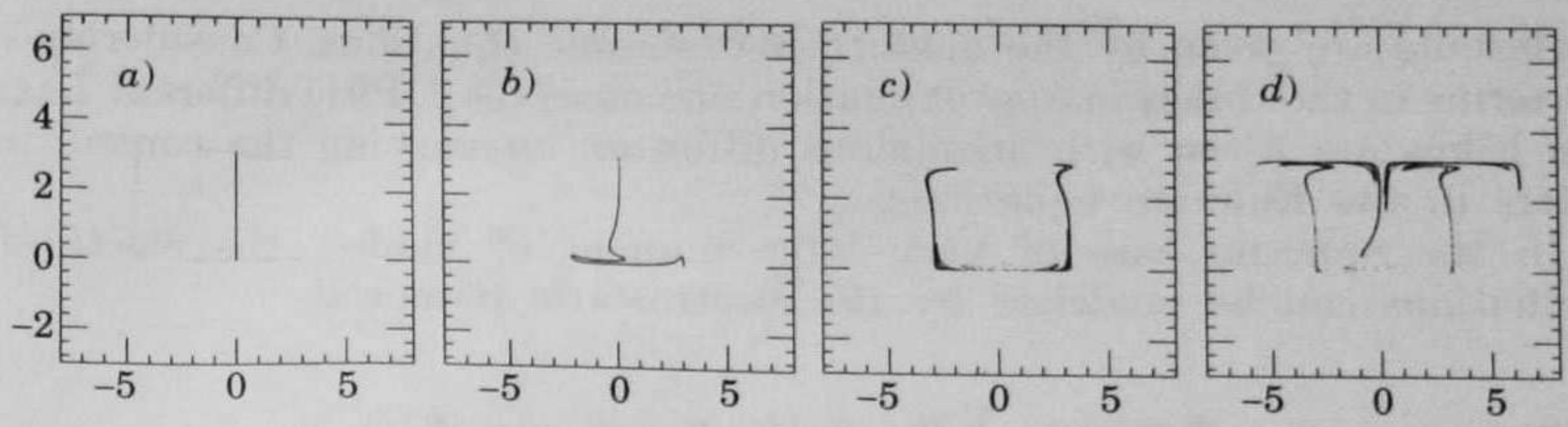

Fig. 20. – A line of 6000 particles, at the initial time (panel *a*)) uniformally distributed on the line $x = 0$ between $y = 0$ and $y = \pi$, is transported according to eqs. (5.7), (5.8) with $A = 0.2$, $B = 0.4$, $\omega = 0.5$, $\lambda = 2\pi$ and $W(y) = \sin y$. Panels *b*), *c*), *d*) show the spreading after, respectively, 2, 4 and 6 periods of the convecting field.

Simple models, as the one just described for the Rayleigh-Bénard convection, can also be applied to the study of charged-particle transport in magnetic-confinement devices. There is, indeed, an exact analogy between the description of the Lagrangian motion of passive tracers in two-dimensional incompressible Eulerian flows and that of charged particles in an electrostatic field with a strong magnetic field. The latter is described by

$$\frac{\mathrm{d}}{\mathrm{d}t}\begin{pmatrix} x \\ y \end{pmatrix} = \frac{c}{B^2}\boldsymbol{E}(\boldsymbol{x},\, t) \times \boldsymbol{B} = \frac{c}{B}\begin{pmatrix} -\partial_y \Phi(x,\, y,\, t) \\ \partial_x \Phi(x,\, y,\, t) \end{pmatrix}, \tag{5.9}$$

where $\Phi(\boldsymbol{x}, t)$ is the electrostatic potential, $\boldsymbol{E} = -\nabla\Phi$ the electric field, $\boldsymbol{B} = B\hat{z}$ the magnetic field and c the light speed. Equation (5.9) is obtained in the limit of electric field varying on frequencies much smaller than the electron and ion gyrofrequencies and in the presence of a strong magnetic field $\boldsymbol{B}$, so that the fast component of charged-particle motion — the Larmor gyration — can be averaged in the so-called guiding-centre approximation [T89]. All these conditions are usually well satisfied in tokamaks. We are then left with a two-degrees-of-freedom Hamiltonian system with $-(c/B)\Phi$ playing the role of the Hamiltonian. Note that (5.9) can also be regarded as the equation of motion of a fluid particle in a two-dimensional Eulerian velocity field given by the stream function $-(c/B)\Phi$.

Observed particle losses in magnetic confinement devices are much stronger than those expected on the basis of pure Coulomb collisions. The origin of such phenomena can reasonably be attributed to a «chaotic advection» of the charged particles driven by the electric field. Lagrangian diffusion of charged particles across a magnetic field has been experimentally detected by laser-stimulated fluorescence of ions in Q-machines [MO87].

Low-frequency electrostatic fluctuations produced by local plasma pressure gradients provide a possible mechanism of enhanced charged-particle transport. Such fluctuations move the particles across magnetic-field lines via the $\boldsymbol{E} \times \boldsymbol{B}$ drift. The effect of a given spectrum of electrostatic fluctuations can be again measured by an effective diffusion coefficient [PVMDOB88].

It is possible to treat the problem with the Galerkin approach, discussed in subsect. **3**·1 and **6**·5. Basically one has to develop Φ in a Fourier series whose

coefficients are given by the magnetohydronamic equations. Considering only few terms in the Galerkin approximation one observes [OP91] different Lagrangian behaviour (even with anomalous diffusion) on varying the control parameters in the Eulerian equations.

In the opposite case of very large number of modes, the electric-field fluctuations can be modelled by the electrostatic potential

$$\Phi(\boldsymbol{x}, t) = \sum_{k} \Phi_k \sin\left[\boldsymbol{k}\cdot\boldsymbol{x} + \phi_k - \omega(\boldsymbol{k})\, t\right]. \tag{5.10}$$

In principle, one should use for $\omega(\boldsymbol{k})$ the dispersion relation for electrostatic driftwaves in order to correctly reproduce the experimental spectrum $S(\boldsymbol{k}, \omega)$. However, this is prohibitive from a computational point of view, so that one is led to the drastic choice $\omega(\boldsymbol{k}) = \omega_0$, a constant. This could be the case for Langmuir waves, but for drift-wave turbulence this is just a simple approximation necessary to make numerical simulations feasible.

Finally the wave number spectrum $|\Phi_k|^2$ is chosen to have a simple power law dependence on k to reproduce the k^{-3} subrange energy spectrum which has been observed in drift-wave turbulence [TFR84]. The ϕ_k are quenched random phases.

A possible form which satisfies the above requirements is

$$\Phi(x, y, t) = \frac{a}{2\pi} \sum_{n,m\in\mathscr{I}} (n^2 + m^2)^{-3/2} \sin\left[\frac{2\pi}{L}(nx + my) + \phi_{nm} - \omega_0 t\right], \tag{5.11}$$

where L is the potential periodicity length in the x and y directions, ϕ_{nm} random phases uniformly distributed in the interval $[0, 2\pi)$ and $\mathscr{I}$ the domain of integration.

The results are better expressed in terms of dimensionless quantities. For this reason we introduce the electric-field strength $\tilde{E} = \langle E^2 \rangle^{1/2}$, where

$$\langle E^2 \rangle = \frac{1}{L^2} \int_0^L \mathrm{d}x \int_0^L \mathrm{d}y\, E^2(x, y, t), \tag{5.12}$$

which can be used as units of electric and magnetic field. By introducing $\hat{\boldsymbol{b}} = \boldsymbol{B}/B$ and $\boldsymbol{e} = \boldsymbol{E}/\tilde{E}$, the equation of motion reads

$$\frac{\mathrm{d}}{\mathrm{d}t}\begin{pmatrix} x \\ y \end{pmatrix} = \frac{2\pi c\tilde{E}}{L\omega_0 B}\boldsymbol{e}(\boldsymbol{x}, t) \times \hat{\boldsymbol{b}} = \mathscr{A}\boldsymbol{e}(\boldsymbol{x}, t) \times \hat{\boldsymbol{b}}, \tag{5.13}$$

where now t, x, y, $\boldsymbol{e}$ and $\hat{\boldsymbol{b}}$ are dimensionless. The parameter $\mathscr{A}$ can be viewed as the ratio of the turbulent drift velocity $v_{\mathrm{d}} = c\tilde{E}/B$ to the maximal phase velocity $v_0 = \omega_0 L/2\pi$.

Numerical simulations [PVMDOB88] show that the effective diffusion coefficient $D = 2(D_{11} + D_{22})$ scales whith $\mathscr{A}$ as, see fig. 21,

$$D \sim \begin{cases} \mathscr{A}^2, & \text{if } \mathscr{A} < 1, \\ \mathscr{A}, & \text{if } \mathscr{A} > 1, \end{cases} \tag{5.14}$$

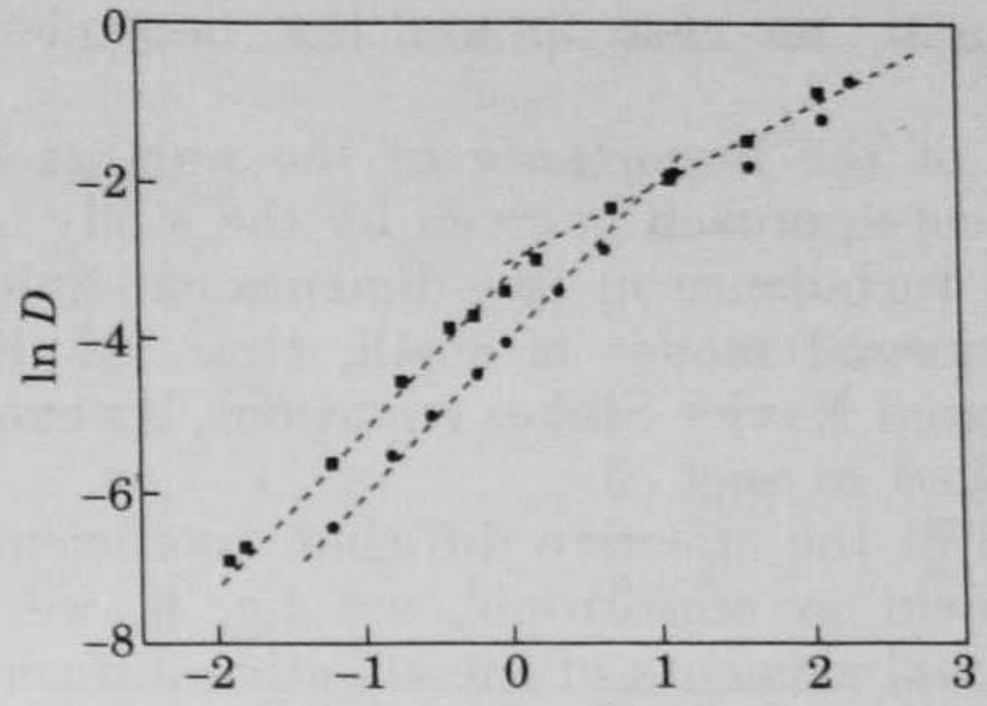

Fig. 21. – Effective diffusion coefficient *vs.* turbulence amplitude parameter $\mathscr{A}$. Full circles refer to model 1, in which only the modes with $n, m = 1, \ldots, N$ and $n^2 + m^2 \leq N^2$ are taken into account. Full squares refer to model 2, in which $n = -N, \ldots, N$, $m = 0, \ldots, N$ and $N_0^2 \leq n^2 + m^2 \leq N^2$.

which are identified with the quasi-linear and Bohm diffusion regime, respectively [K84]. This result does not depend on the form of $\mathscr{I}$, so that the system exhibits a quite good «structural stability».

The power law (5.14) can be obtained with a simple analytical approach by using some ideas of the closure approximation of turbulence [L73]. Under the hypothesis that the position of a test charged particle is a Gaussian process statistically independent of the electric field, it is possible to write a close equation for $\langle (\boldsymbol{x}(t) - \langle \boldsymbol{x}(t) \rangle) \rangle$. The solution of this equation shows the power law (5.14). The reader can find the details in [PVMDOB88].

The power law (5.14) can also be obtained with a naive dimensional analysis. For any fixed time t we can draw the equipotential curves of the electric field. For time-independent potential the charged particles will move according to the equipotential curves. However, the latter are oscillating in time with a frequency ω. As a consequence, a particle which is moving according to a given equipotential curve has a finite probability of being «trapped» in a finite time by another equipotential curve. Assuming that the motion in the two equipotential curves is uncorrelated, reasonable assumption due to the chaotic nature of the motion, the effective diffusion coefficient can be obtained as $D \sim v_d^2 \tau$, since v_d is the typical particle velocity on an equipotential curve, and τ is the typical «permanence» time on an equipotential curve. Without loosing in generality we can assume $v_0 \simeq 1$, so that $v_d = \mathscr{A}$. For the typical time we are left with two possible choices, $\tau_0 = 2\pi/\omega_0$ and $\tau_d \sim 1/A$. Thus we have $D \sim v_d^2 \min(\tau_0, \tau_d)$ which yields to $D \sim \mathscr{A}^2$ for $\mathscr{A} < 1$ ($\tau_0 < \tau_d$) and $D \sim \mathscr{A}$ for $\mathscr{A} > 1$ ($\tau_0 > \tau_d$).

The above result, and the subsequent dimensional analysis, may lead to the wrong conclusion that things are simple. In fact, here the basic ingredient that makes the «statistical» approach meaningful is that there are many k. The situation is similar to that of fully developed turbulence where there are excitations on a wide range of scales. However, we know that near the transition to turbulence, where the number of excited k is small, things are quite different. In fact if we take few waves in (5.10) relation (5.14) ceases to be

correct and, in general, no clear power law dependence of D on $\mathscr{A}$ appears [KD84].

A clear example of the importance of the number of normal modes for a meaningful statistical approach is given by the study of diffusion properties near the transion to turbulence in two-dimensional fluid. In this regime the number of excited normal modes is small, thus the Eulerian field can be represented by truncated Navier-Stokes equations. As example we consider the 5-modes system studied in sect. **3**.

We are interested in the effective diffusion coefficient in the range $\varepsilon > \varepsilon_c$. Since the Eulerian field in anisotropic, see fig. 8, we define two diffusion coefficients (the diagonal elements of the effective diffusion tensor D_{ij}) D_x and D_y as

$$\begin{cases} D_x = \lim_{\tau\to\infty} \frac{1}{2\tau} \overline{(x(t+\tau) - x(t))^2}\,, \\ D_y = \lim_{\tau\to\infty} \frac{1}{2\tau} \overline{(y(t+\tau) - y(t))^2}\,, \end{cases} \tag{5.15}$$

where $\overline{(\ldots)}$ is a temporal average over a very long time.

Naive arguments could be used to relate $D_{x,y}$ to the maximum Lyapunov exponents λ_L of the Lagrangian motion. By assuming for chaotic motion a finite uncorrelation time $\tau_u \sim 1/\lambda_L$, we have $D_{x,y} \sim L^2/\tau_u$, *i.e.*

$$D_{x,y} \sim \lambda_L\,, \tag{5.16}$$

assuming that L — the typical distance the particle runs in a time τ_u — does not depend on Re.

A different appraoch makes use of the Kubo formula

$$D_i = \int_0^\infty \mathrm{d}\tau\, \overline{v_i(t+\tau)\, v_i(t)} \sim \overline{v^2}\tau_d \sim \overline{v^2}/\lambda_L\,, \qquad i = x,\ y\,, \tag{5.17}$$

where we have made the likely choice $\tau_d \sim 1/\lambda_L$ for the typical correlation decay time.

Numerical computations of $D_{x,y}$, however, show that simple relation like (5.16) or (5.17) between $D_{x,y}$ and λ_L does not exist. Indeed when ε increases D_x first decreases and then increases. On the contrary D_y always increases with ε [FV89], see fig. 22. The above-mentioned statistical arguments, which give good results for the diffusion of charged particles in a turbulent plasma, are inadequate in the present situation even on a qualitative level . The origin of this failure is the fact that when $\varepsilon \sim O(1)$ the autocorrelation function of $\dot{x} \equiv v_x$ decays on times much larger than $1/\lambda_L$. The motion is chaotic, but with a well-defined structure. The horizontal diffusion for $\varepsilon \gtrsim \varepsilon_c$ is ruled by the intervals of regular motion. There is no similarity with the standard diffusion in the Brownian motion. This case resembles a random walk with a probability distribution of pausing times between successive steps in the walk [MS84]. Roughly speaking, here we have the following scenario: regular ballistic motion in the x-direction for a certain time interval — which diverges as $\varepsilon \to \varepsilon_c^+$

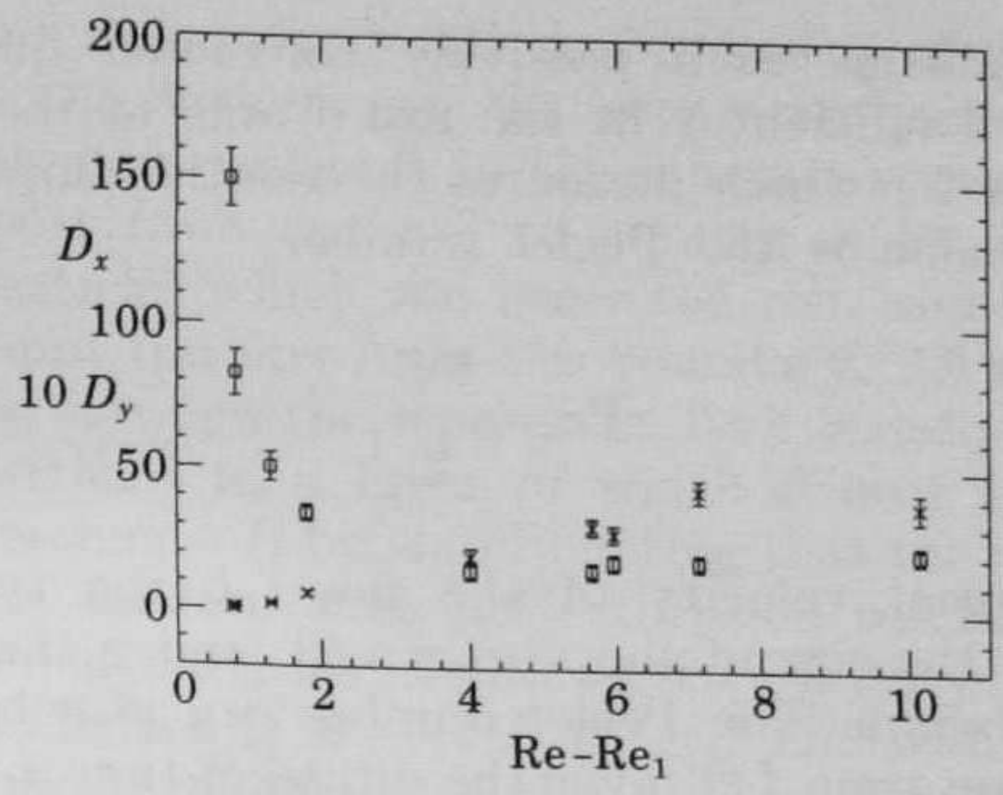

Fig. 22. – Diffusion coefficients D_x(□) and $10D_y$(×) as functions of $\mathrm{Re} - \mathrm{Re}_1$, for particles convected by the 5-modes truncation of the Navier-Stokes equations.

— entrapping inside a small region of highly chaotic motion, and then ballistic motion but not necessarily in the same sense of the preceding one, fig. 23. This implies a strong correlation of v_x which decays on times much larger than $1/\lambda_L$, and hence a large value of D_x for $\varepsilon \sim \varepsilon_c^+$ (see (5.17)].

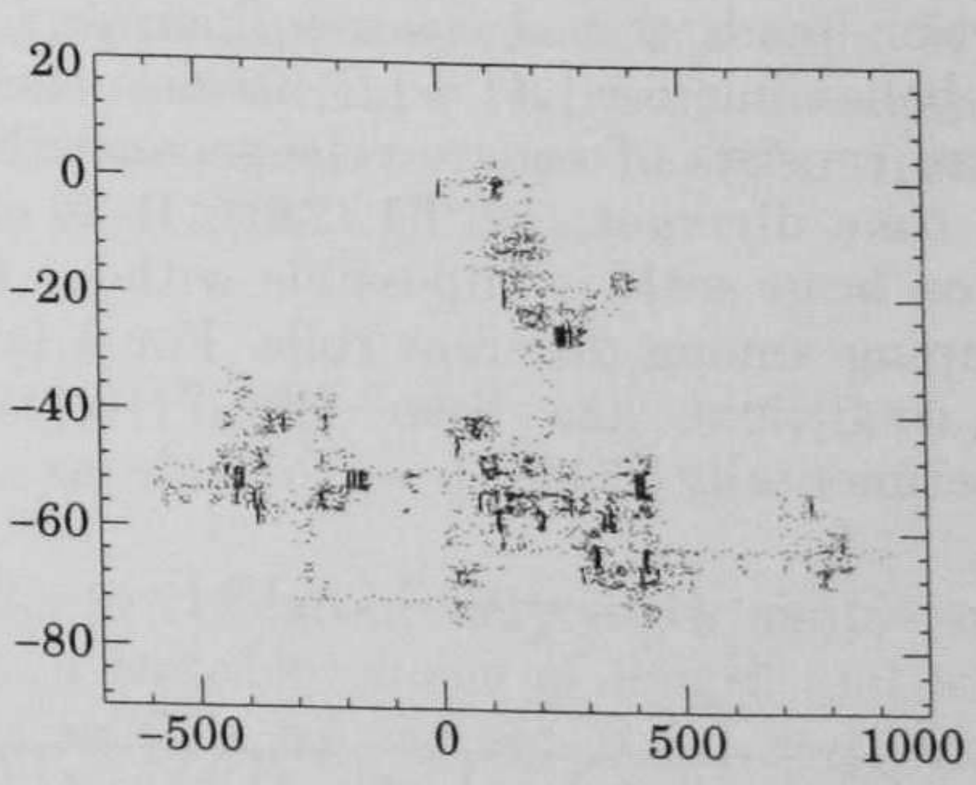

Fig. 23. – 5000 positions of a particle driven by the equations of the 5-modes model with $\mathrm{Re} - \mathrm{Re}_1 = 1.3$, taken every unit of natural time.

5·2. *Diffusion in steady velocity fields.* – In the above examples the diffusion of impurities was entirely due to Lagrangian chaos. The molecular diffusion played no role. Real fluids, however, always have a (small) degree of molecular diffusion. For this reason it is interesting to study the opposite extreme case, *i.e.* the effect of a small molecular diffusion on simple integrable Eulerian velocity fields. In the case of two-dimensional velocity fields this corresponds to time-independent stream functions. This problem is of interest in both fluids and plasmas where two-dimensional laminar flow patterns are encountered as stationary states of driven systems. Classical examples are the two-dimensional rolls of the Rayleigh-Bénard problem and the Taylor vortices in the Couette flow and heat flow in a convecting fluid.

In all these problems each passively convected quantity has its own molecular diffusion coefficient χ in the rest frame of the fluid. The relevant dimensionless parameter which measures the relative importance of advection over molecular diffusion is the Peclet number

$$\mathrm{Pe} = \frac{VL}{\chi}, \tag{5.18}$$

where V is the typical velocity of the flow, L the typical length of the convective flow, *e.g.* the size of the vortex cell, and χ the molecular diffusion coefficient of the medium. The Peclet number can also be understood as the ratio of the convection time L/V over the diffusion time L^2/χ across a distance L.

The physical interesting case is when the convective transport exceeds substantially the diffusion transport, *i.e.* for large Peclet numbers. In this context we shall analyse a widely studied two-dimensional convective velocity field given by the projection of the ABC flow with $C = 0$ on the (x, y)-plane

$$\boldsymbol{u} = (B \cos y,\ A \sin x)\,, \tag{5.19}$$

whose stream function reads $\psi = A \cos x + B \sin y$.

The qualitative behaviour for $|A| = |B|$ models the Rayleigh-Bénard convection, as the phase consists of square cells separated by lines (separatrices) where the rotation time diverges, see fig. 24*a*). It is clear that dispersion of a passive impurity on large scale is impossible without the molecular diffusion that allows the jumping among different rolls. For a large Peclet number the effective diffusion coefficient has been found — theoretically [P85, S87, RBDH87] and experimentally [SG88b] — to scale as

$$D_{ij} \sim \chi \mathrm{Pe}^{1/2} \sim \chi^{1/2}\,. \tag{5.20}$$

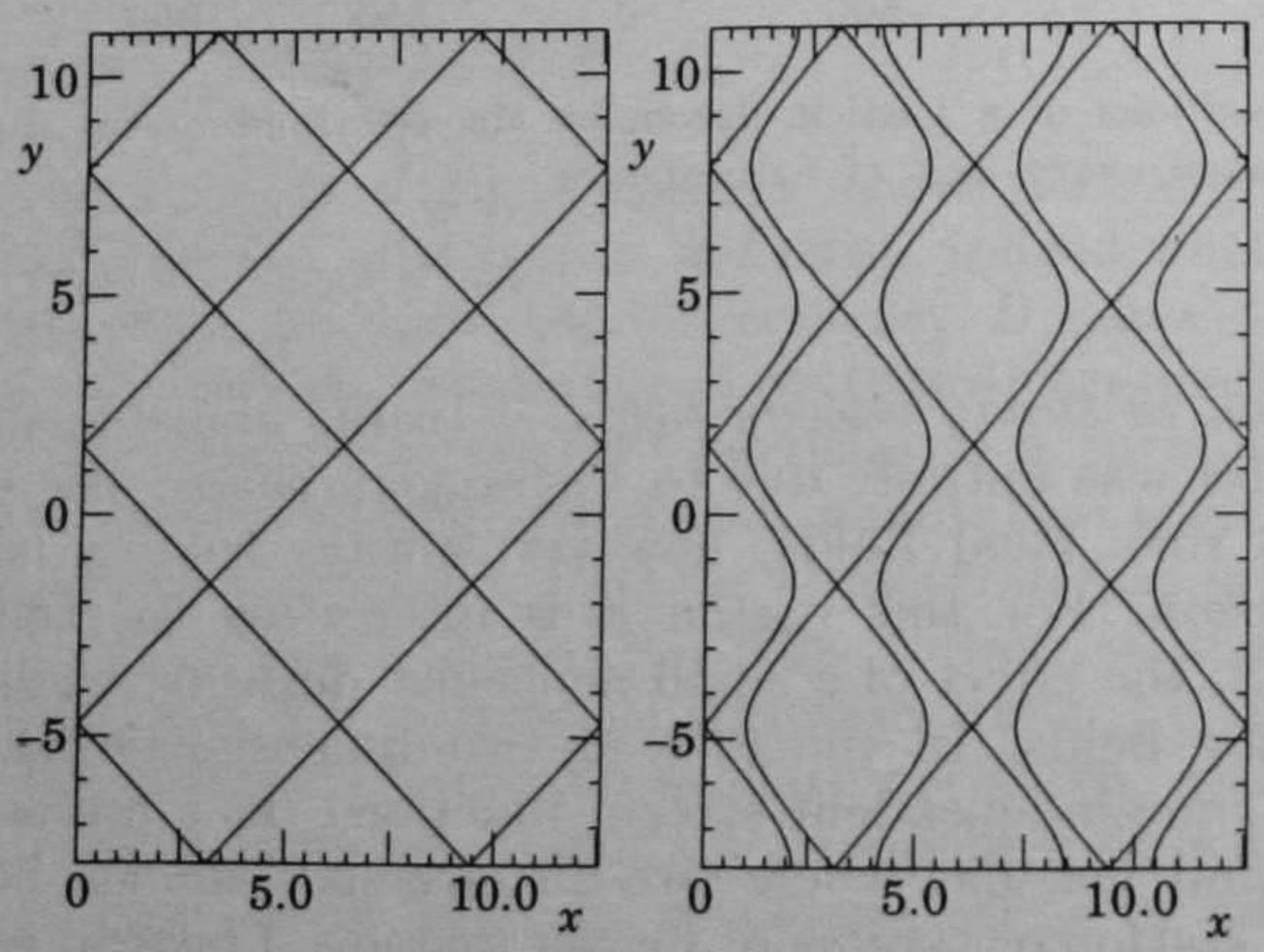

Fig. 24. – Structure of the separatrices of eq. (5.3), for the field (5.19); case *a*) is with $A = -1$, $B = 1$; case *b*) with $A = -1.3$, $B = 1$.

D_{ij} is thus much larger than χ for $\chi \to 0$. A simple way of understanding (5.20) is the following. In the vicinity of the separatrix between two rolls the component of the flow perpendicular to the separatrix vanishes, and the only mechanism of transport from one roll to another is by molecular diffusion. Therefore the only particles which can leave the roll, and hence contribute to transport, are those «not too far» from the boundary. All the others have not enough time to diffuse through the separatrix. As a consequence, the transport is entirely due to particles in a layer of width δ near the separatrix. This scenario allows us to estimate D by simply noting that the particles close to the separatrices perform a random walk with diffusion coefficient $\sim L^2/\tau$, where $\tau = L/V$. The fraction of particles in the «active» layer is $\sim \delta/L$, so that the effective diffusion coefficient is $D \sim (\delta/L)(L^2/\tau)$. The width δ depends on the molecular diffusion, and is roughly given by $\delta^2 \sim \chi\tau$. This immediately leads to the conclusion that the effective diffusion coefficient scales as $D \sim \chi \mathrm{Pe}^{1/2}$. This result can be obtained in a more rigorous way, the interested reader is referred to references.

When $|A| \neq |B|$, narrow channels arise among the convective cells, in a direction which depends on the relative magnitude of $|A|$ and $|B|$, see fig. 24*b*). The motion of test particles inside a channel appears to be ballistic and this enormously enhances the transport along the channel direction. The process is strongly anisotropic and can be regarded as due to long runs in the channel interrupted by trapping periods inside the rolls. It is useful to introduce two effective diffusion coefficients, $D_{\parallel}$ along the channels direction and $D_{\perp}$ along the direction transversal to the channels. In the limit of small molecular diffusion one has [CS89, CFPV90a]

$$(5.21) \qquad D_{\parallel} \propto \frac{L^2}{V} \big||A| - |B|\big|^3 \chi^{-1} \quad \text{and} \quad D_{\perp} \propto V \big||A| - |B|\big|^{-1} \chi .$$

As in the case $|A| = |B|$, (5.21) can be derived by simple arguments. Without losing in generality, by a suitable choice of length and time units, we have $L = O(1)$ and $V = O(1)$ so that we can set $B = 1$ and $A = -(1 + \delta)$. In the following our dimensional arguments neglect multiplicative factors $O(1)$, such as L and V. The stream function becomes $\psi = \sin y - (1 + \delta)\cos x$, which for $\delta = 0$ describes convection cells of width 2π, where in the absence of a noise term the motion of a test particle is always periodic. The separatrices are the lines where the stream function is zero (for $\delta = 0$) and they cross at the unstable hyperbolic fixed points of the flow. When $\delta > 0$ the border lines between cells do not coincide and there appear channels along the y-direction, see fig. 24. By simple perturbative calculations one finds that for small δ the width of a channel is $\sim \delta$, although the maximum distance between the separatrices increases up to $\sim \delta^{1/2}$ near the unstable fixed points. Note that $\delta < 0$ corresponds to channels along the x-axis. The motion of a particle inside the channels, neglecting molecular diffusion, is ballistic and the velocity field changes sign between neighbour channels. For small χ, a test particle can jump into a channel, because of molecular diffusion. Then, one has a ballistic motion inside the channel with velocity $V_c \sim O(1)$ either in the up or in the down y-direction stopped by a capture from a cell after a time $T_c \sim \delta^2/\chi$, and so on.

Let us consider the case for which

$$T_c/T_r \gg 1, \quad i.e. \quad \delta^2/\chi \gg 1,$$

since the circulation time $T_r \sim V/L \sim O(1)$. This dimensional estimate of the diffusive times in the channels allows to compute the effective diffusivity tensor which in these coordinates is diagonal with $D_\perp = D_{11}$ and $D_\parallel = D_{22}$. The typical length of a run along a channel is

$$L_c \sim T_c V_c \sim \delta^2/\chi . \tag{5.22}$$

The probability p to find a particle in a channel is proportional to its width $\sim \delta$, and thus we obtain

$$D_\parallel \sim p \frac{L_c^2}{T_c} \sim \frac{\delta^3}{\chi} . \tag{5.23}$$

On the other hand, the transport in the x-direction can be described as a random walk where the time step is T_c and the length step is the cell width $\sim 2\pi$. This leads to

$$\frac{\langle (x(t) - \langle x \rangle)^2 \rangle}{4\pi^2} \propto p \frac{t}{T_c} , \tag{5.24}$$

so that

$$D_\perp \sim \frac{\chi}{\delta} . \tag{5.25}$$

These arguments are valid only in the limit of large T_c/T_r. By this we mean that the time spent in the channels should be large with respect to the circulation time T_r, *i.e.* $\chi \ll \delta^2$. When T_c/T_r becomes smaller than unity, a particle has not enough time to perform a significant run along a channel between two successive trappings. Practically the transport process can be described as if there were no channels. In this limit, $\chi \to 0$, $\delta \to 0$, with $T_c/T_r \sim 1$, the anisotropy disappears and one recovers the $|A| = |B|$ scaling (5.20)

$$D_\parallel \sim D_\perp \propto (VL)^{1/2} \chi^{1/2} . \tag{5.26}$$

The agreement with the numerical data is very good for $D_\parallel$, but only fair for $D_\perp$, see fig. 25 and 26. This because the above scaling arguments do not consider the additional linear term in χ due to the bare molecular diffusion. We stress that in spite of the apparently «anomalous» diffusion process — long runs interrupted by trappings — the kurtosis tends to the Gaussian value 3 so that the diffusion is standard and Gaussian.

The situation here is similar to the one discussed for the truncated Navier-Stokes equations [FV89]. There the «jumping» was due to the Lagrangian chaos, here to the molecular diffusion. However, the physical mechanisms

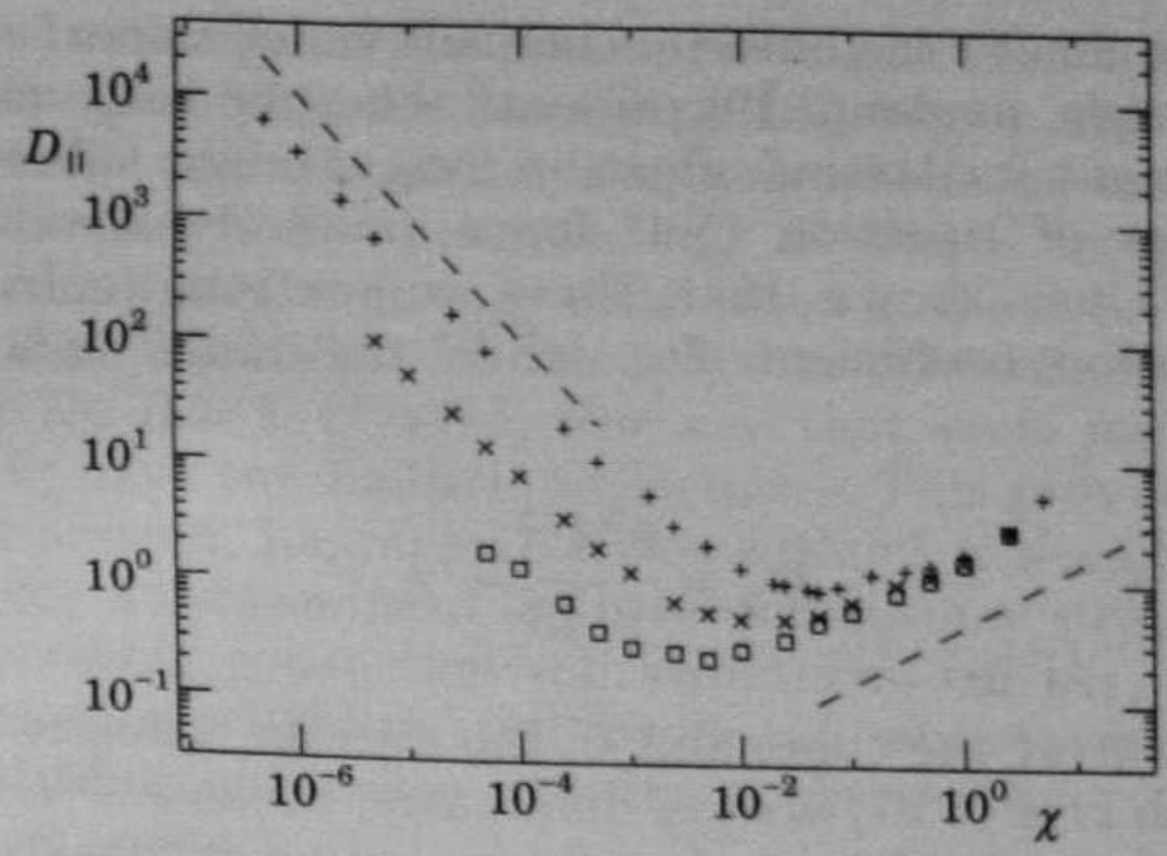

Fig. 25. – The longitudinal diffusion coefficient *vs.* the molecular diffusion coefficient for the field (5.19) and: $|A| - |B| = 0.30$ (+), 0.15 (×), 0.075 (□). The (dashed) lines with slopes -1 and $1/2$ are drawn for comparison. The numerical errors bar are comparable with the symbols size.

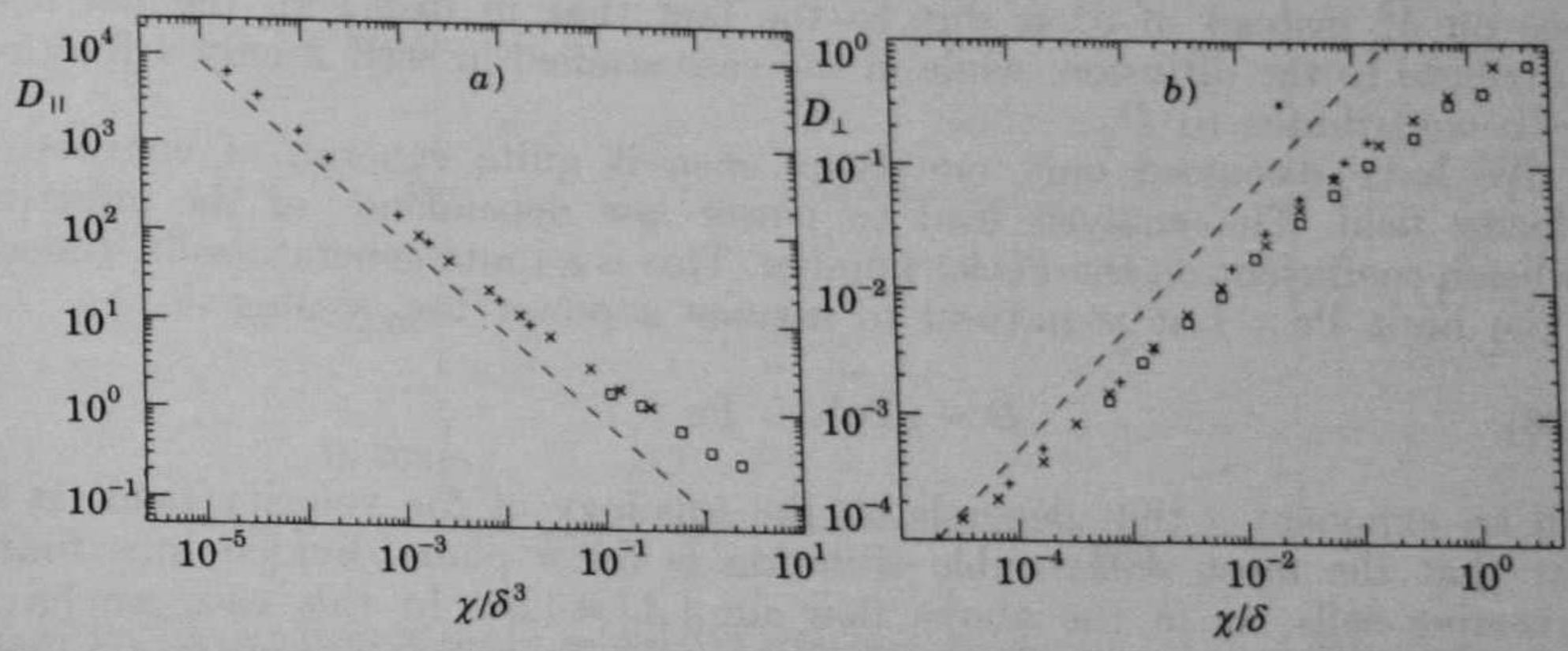

Fig. 26. – *a*) The longitudinal diffusion coefficient *vs.* χ/δ^3 (together with a dashed line of slope -1). *b*) The transverse diffusion coefficient *vs.* χ/δ (together with a dashed line of slope 1). The symbols refer to $\delta = |A| - |B| = 0.30$ (+), 0.15 (×), 0.075 (□). The numerical errors bars are comparable with the symbols size.

which rule the diffusion is the same. The tracer is trapped for long times in a small limited region of space and then escapes along ballistic channels until a subsequent trap. Indeed, the qualitative behaviour of the effective diffusion coefficient is found to be the same as the one given by the Langevin equation: the longitudinal diffusion coefficient diverges approaching ε_c, as $D_{\|} \propto (\varepsilon - \varepsilon_c)^{-a}$; while the transversal diffusion coefficient vanishes as $D_\perp \propto (\varepsilon - \varepsilon_c)^a$, with $a \approx 1/2$. In a rough way, eq. (5.1) with an integrable velocity field can be regarded as a crude approximation of a Lagrangian chaotic system described by eq. (5.3). In this sense, the perturbation strength $(\varepsilon - \varepsilon_c)^a$ plays the role of the noise variance χ.

The above analysis was performed for two-dimensional systems, however it is easy to realize that similar behaviours may be also found in three-dimen-

sional ones. This is due to the ballistic channels which appear in a large class of systems. For example, model (5.19) presents the same behaviour as the dispersion of a contaminant for laminar flows in long straight tubes or channels. By the direct analysis of equation (5.4) for a passively advected scalar field, Taylor [T53, T54] has shown that there is a strong enhancement of the longitudinal diffusion coefficient $D_{\parallel}$, while the radial inhomogeneities are smoothed out:

$$D_{\parallel} = \frac{\hat{\delta}^2 U^2}{\chi} \frac{}{48} + \chi , \tag{5.27}$$

where $\hat{\delta}$ is the radius of the tube, and U the average velocity of the flow. The first term of the r.h.s. of (5.27) always dominates, because $\hat{\delta}^2 U^2/\chi^2$ is very large ($\gg 1$), except for the case of very slow flows and/or extremely fine capillaries. The presence of transverse velocity gradients causes the sharp increase of $D_{\parallel}$. It is worth stressing that the larger the molecular diffusion the smaller the longitudinal dispersion. It is not difficult to understand that the leading term in (5.27) can be obtained by the arguments discussed in sect. **2**. The dependence on $\hat{\delta}^2$ instead of δ^3 is due to the fact that in (5.27) all the particles contribute to the diffusion, while in the case studied in sect. **2** only a fraction $p \sim \delta$ contributes to $D_{\parallel}$.

We have discussed only one type, even if quite general, of convective velocity field. The analysis lead to power law dependence of the effective diffusion coefficient on the Peclet number. This is a quite general result. Indeed in the limit $\mathrm{Pe} \gg 1$ it is natural to assume a power law scaling

$$D \sim \chi \mathrm{Pe}^{\alpha}, \quad \mathrm{Pe} \gg 1 , \tag{5.28}$$

with an exponent α that depends on the topology of the velocity field. It is clear that the most unfavorable situation is for a plane divided into finite convective cells, as in the above flow for $|A| = |B|$. In this case we have $\alpha = 1/2$. The other extreme case is when there is a finite fraction of stream lines which go to infinity in some directions, *e.g.*, the channels in the above example. In this case $\alpha = 2$. Therefore, from a physical point of view, we expect $1/2 \leq \alpha \leq 2$. For example, in the so-called «common-position» case [IKTTY89] found $\alpha = 10/13$.

Recently rigorous results on the effective diffusion coefficient in periodic flows were obtained on a general ground by Kalugin *et al.* [KST90]. They studied the analytical properties of the effective diffusion coefficient D_n for a given direction n as a function of Pe and found that

$$\chi < D_n < \chi(1 + \mathrm{const}\,\mathrm{Pe}^2) \quad \text{for} \quad \forall n, \ \forall \mathrm{Pe} . \tag{5.29}$$

The left-hand side of this formula means that the presence of the flow increases the diffusivity, while the right-hand side leads to the important conclusion that the effective diffusion coefficient is bounded from above. Moreover, this implies that if D_n has a scaling behaviour (5.28) for large Peclet numbers, then the critical index α should be in the interval [0, 2]. The actual value depends, of course, on the geometry of the velocity field.

The presence of molecular diffusion can also have a nontrivial role in three-dimensional steady space-periodic flows with Lagrangian chaos. This is due to the regular trajectories along ballistic directions which appear in generic three-dimensional chaotic flows. For instance, fig. 27 shows the positions of 1000 particles, which are initially uniformly distributed in the cube $(0,2\pi) \times (0,2\pi) \times \times (0,2\pi)$, after a time $t = 10\,000$ for the full three-dimensional ABC flow with parameters $A = 1.15$, $B = 1$, $C = 0.1$. One sees that some particles (spots very far from the origin) have run ballistic trajectories. This provides evidence that, for every initial condition, Lagrangian chaos without molecular diffusion is not sufficient to disperse a contaminant in three-dimensional steady velocity fields, such as those describing convection roll structures. On the contrary, without a molecular diffusion mechanism, the dispersion of contaminants is obtained for all initial conditions only when velocity fields are time dependent, both in two and thre dimensions.

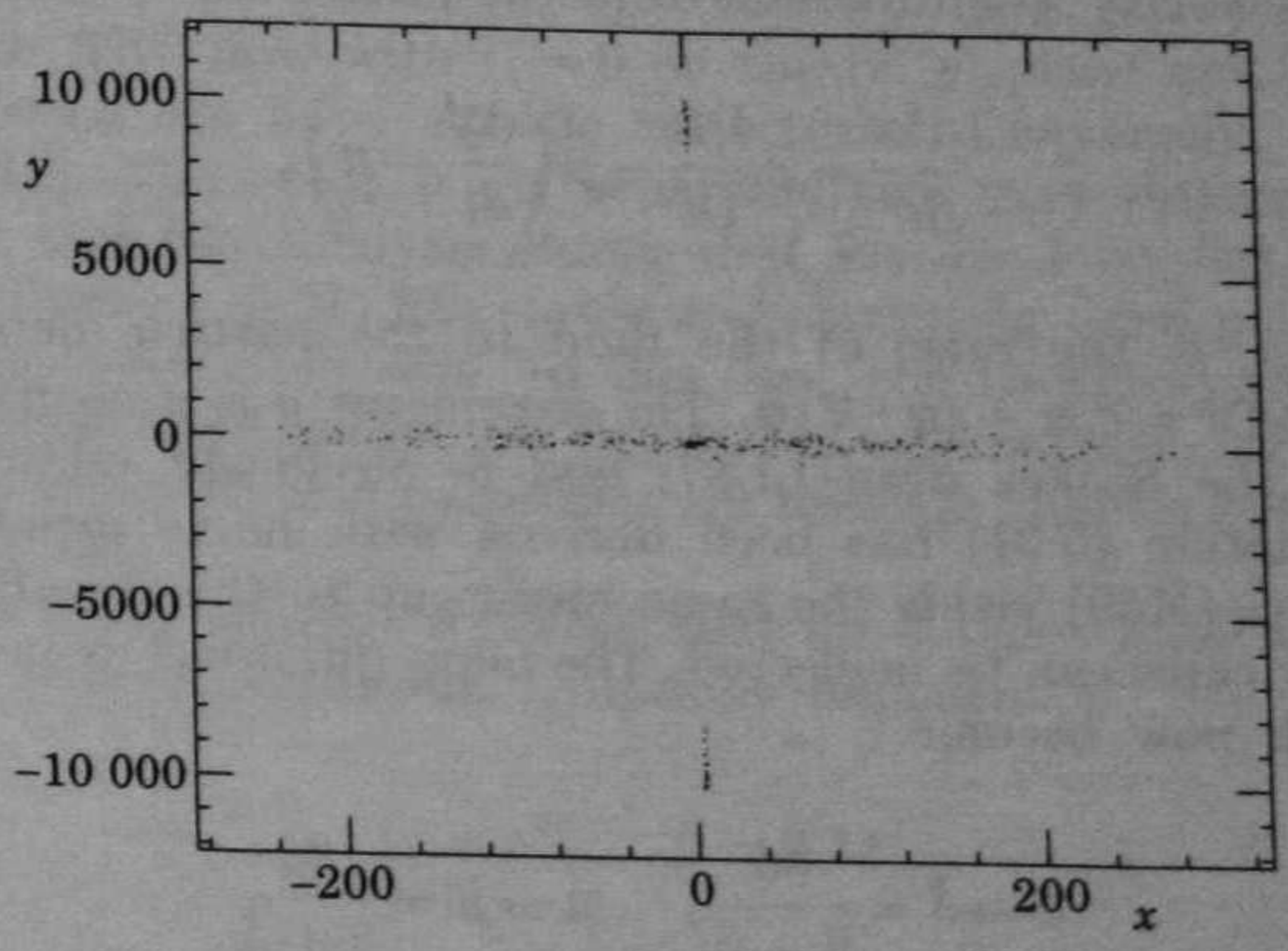

Fig. 27. – The positions in the (x, y)-plane of 1000 particles, initially in a cube of side 2π at the origin of the axes, after they evolved for 10 000 units of time according to the $3d$ ABC flow, with parameters $A = 1.15$, $B = 1.0$ and $C = 0.1$.

5·3. *Diffusion of particles denser than the fluid.* – In the cases studied up to now the particles have the same density of the fluid, *i.e.* they are «fluid particles». We conclude this section by considering the diffusion properties of particles whose density differs from the fluid density [CFPrV90]. The interesting result is that in this case chaotic behaviour and standard diffusion properties may be observed also for velocity fields for which the «fluid particles» follow regular orbits, without undergoing any diffusion process, *i.e.* for regular solution of (5.3). Since this behaviour is generated by the density difference between the passive test particles and the fluid particles, this type of diffusion has been called «inertial diffusion». There exist few studies of the chaotic behaviour of these systems [YGO90, WBS90, WBS91], which however do not consider the diffusion properties.

The starting point for the study of chaotic advection was (5.3). In the